

On the Peril of Inferring Phytoplankton Properties from Remote-Sensing Observations

J. Xavier Prochaska^{1,2,3,4*}, Robert J. Frouin⁴

¹Affiliate of the Ocean Sciences Department, University of California, Santa Cruz

²Department of Astronomy & Astrophysics, University of California, Santa Cruz

³Kavli IPMU

⁴Scripps Institution of Oceanography, University of California, San Diego

arXiv:2408.06149v1 [physics.ao-ph] 12 Aug 2024

*Current address, Scripps Institution of Oceanography

Corresponding author: J. Xavier Prochaska, jxp@ucsc.edu

Abstract

Remote-sensing satellites are the only means to observe the entire ocean at high temporal cadence. Since 1978, sensors have provided multi-band images at optical wavelengths to assess ocean color. In parallel, sophisticated radiative transfer models have been developed to account for attenuation and emission by the Earth’s atmosphere and ocean, thereby estimating the water-leaving radiance or and remote-sensing reflectance $R_{rs}(\lambda)$. From these $R_{rs}(\lambda)$ measurements, estimates of the absorption and scattering by seawater are inferred. We emphasize an inherent, physical degeneracy in the radiative transfer equation that relates $R_{rs}(\lambda)$ to the absorption and backscattering coefficients $a(\lambda)$ and $b_b(\lambda)$, known as inherent optical properties (IOPs). This degeneracy arises because $R_{rs}(\lambda)$ depends on the ratio of b_b to a , meaning one cannot retrieve independent functions for the non-water IOPs, $a_{nw}(\lambda)$ and $b_{b,nw}(\lambda)$, without a priori knowledge. Moreover, water generally dominates scattering at blue wavelengths and absorption at red wavelengths, further limiting the potential to retrieve IOPs in the presence of noise. We demonstrate that all previous and current multi-spectral ocean color satellite observations lack the statistical power to measure more than three parameters total to describe $a_{nw}(\lambda)$ and $b_{b,nw}(\lambda)$. Due to the ubiquitous exponential-like absorption by color dissolved organic matter (CDOM), detritus, and non-pigmented biomass at short wavelengths ($\lambda < 500$ nm), multi-spectral $R_{rs}(\lambda)$ do not permit the detection of phytoplankton absorption $a_{ph}(\lambda)$ without very strict priors. Furthermore, such priors lead to biased and uncertain retrievals of $a_{ph}(\lambda)$. Hyperspectral observations may recover a fourth and possibly fifth parameter describing only one or two aspects of the complexity of $a_{ph}(\lambda)$. These results cast doubt on decades of literature on IOP retrievals, including estimates of phytoplankton growth and biomass. We further conclude that PACE will greatly enhance our ability to measure the phytoplankton biomass of Earth, including its geographic and temporal variations, but challenges remain in resolving the IOPs.

1 Introduction

Phytoplankton play essential roles within our ecosystem, serving as the base of the ocean food web and performing $\sim 50\%$ of all photosynthesis on Earth. Therefore, assessing phytoplankton growth and death – especially in a changing climate (Behrenfeld et al., 2016; Flombaum et al., 2020) – is critical to any effort to track and predict the health of our planet. Decades of phytoplankton research have revealed significant regional variations in these process and demonstrated that phytoplankton are highly dynamic on relatively short time scales (hours to weeks, especially in coastal areas, due to tides, upwelling, pulses of freshwater inflow, and other episodic events (e.g. Cloern & Jassby, 2010)). To identify any long-term trend, therefore, one must first develop a detailed picture of the variations on seasonal and shorter timescales.

Unfortunately, our ability to measure phytoplankton in-situ is greatly hampered by the vast expanse of the ocean. Measurements with high temporal frequency can only be acquired at select, fixed stations such as OceanSITES (Boss et al., 2022). Therefore, oceanographers have turned to remote-sensing satellite observations to perform high-cadence, global analyses of the ocean surface. Beginning with the Coastal Zone Color Scanner experiment (Hovis et al., 1980), multi-band observations in optical channels have enabled the inference of the concentration of phytoplankton and other seawater constituents, e.g. colored dissolved organic matter (CDOM) and detritus. These inferences are retrieved from satellite-derived remote sensing reflectance $R_{rs}(\lambda)$, which represents the water-leaving radiance normalized by incident solar irradiance. These are defined and recovered by their absorption and backscattering coefficients $a(\lambda)$, $b_b(\lambda)$, so-called inherent optical properties (IOPs).

The underlying physics for IOP retrievals is radiative transfer: the absorption and scattering of sunlight by seawater modulates and directs incident sunlight back to the

satellite. While the radiative transfer physics is straightforward (but not simple; C. D. e. Mobley, 2022), there are many factors that complicate the calculations. These include but are not limited to: the concentration of the constituents (typically the desired unknown), their variation with depth, the precise wavelength dependence of the absorption and scattering coefficients of each constituent, geometric factors associated with the Sun’s location relative to the satellite. In addition, Earth’s atmosphere attenuates the signal and introduces a dominant background radiation field which must first be estimated and subtracted (“corrected”) which fundamentally limits the precision of any space-based $R_{rs}(\lambda)$ estimation.

For decades, researchers have attacked this radiative transfer problem to attempt retrievals of scientifically valuable quantities including an estimate of the phytoplankton biomass. There is a robust and well-founded literature describing (and performing) the translation of so-called apparent optical properties (AOPs, e.g. $R_{rs}(\lambda)$) to inherent optical properties (IOPs; $a(\lambda)$, $b_b(\lambda)$) that depend solely on the water constituents and the water itself. Ideally, one first parameterizes and then estimates (“retrieves”) the absorption and backscattering spectra of the non-water component $a_{nw}(\lambda)$, $b_{b,nw}(\lambda)$ and then infers concentrations of phytoplankton, CDOM, detritus, etc. From these, one may examine the geographic distribution and temporal evolution of fundamental biological processes across the global ocean (Fox et al., 2022).

During the development of a diverse set of IOP retrieval algorithms for this purpose (see Werdell et al., 2018, for a review), the ocean optics community has acknowledged key challenges to the problem largely independent of those associated with radiative transfer. These include uncertainties related to the atmospheric corrections, non-uniqueness between common constituents (e.g. CDOM and detritus), and retrieving multiple unknowns from limited datasets (e.g. multi-spectral observations). A few, sparsely-cited works have also highlighted a far more fundamental obstacle to the process: a physical “ambiguity” in the inversion of the radiative transfer equation (Sydor et al., 2004; Defoin-Platel & Chami, 2007). Unfortunately, this problem has often been confused or conflated with the statistical limitations of an insufficient number of bands measuring $R_{rs}(\lambda)$ (Werdell et al., 2018; Cetinić et al., 2024). As such, while the community has acknowledged challenges to IOP retrievals from remote-sensing observations, rigorous assessment of the algorithms themselves has been limited and usually only performed in the context of comparisons to sparse, in-situ observations (e.g. Lee, 2006; Seegers et al., 2018).

Another fundamental aspect of the problem is that we do not know the optimal basis functions that describe $a(\lambda)$ and $b_b(\lambda)$ nor even the complete set (Garver et al., 1994). Indeed, it is an aspiration within the ocean color field to recover (or even discover) the composition of phytoplankton (e.g. Mouw et al., 2017). The ocean color research community has hoped that the main limitation is the sparsity of existing multi-spectral bands provided by current satellites and that hyperspectral observations will lead to a major breakthrough. Indeed, Cael et al. (2023) has demonstrated from a data-driven analysis of $R_{rs}(\lambda)$ data its limited information content, i.e. only ~ 2 degrees-of-freedom in multi-spectral, satellite observations. But they also concluded that in-situ hyperspectral datasets offer only one or two additional degrees of freedom. In this manuscript, we examine this question from a new angle – with the standard approach of IOP retrievals – and reach similar conclusions.

Here, we introduce the Bayesian Inferences with Gordon coefficients (BING) package for ocean retrievals in a Bayesian context. Our approach follows many of the standard assumptions of widely adopted algorithms in the literature, e.g. the generalized IOP (GIOP) model (Werdell et al., 2013), the Garver-Siegel-Maritorena (GSM) algorithm (Maritorena et al., 2002). In addition, we emphasize and expand upon the “ambiguity” problem – a physical degeneracy in the radiative transfer equation that couples reflectances to IOPs – which fundamentally limits IOP retrievals. In turn, we demonstrate that IOP

retrievals from multi-spectral datasets constrain at most three parameters describing $a_{nw}(\lambda)$ and $b_{b,nw}(\lambda)$. Therefore, if one allows for the fact that the spectral shape of CDOM absorption varies and is unknown, then we show one cannot retrieve a measurement of phytoplankton absorption. This includes all previous missions with satellites carrying multi-bands sensors. We then examine the prospects for IOP retrievals with hyperspectral observations and discuss additional opportunities to address the deep degeneracies that lurk within.

2 The Bad: A physical degeneracy in the radiative transfer

At the heart of our analysis is a new Bayesian inference algorithm for the retrieval of IOPs from remote sensing reflectances, the BING package. The primary motivations for introducing a Bayesian framework are twofold: (i) it forces one to explicitly describe all of the priors that influence the result; and (ii) it permits well-established approaches for performing model selection, i.e., estimating the maximum number of free parameters one can use to describe the data.

To construct any such algorithm, one must have a well-defined forward model to predict the observables, here remote-sensing reflectances $R_{rs}(\lambda)$. For IOP inversion, this means a radiative transfer model – or its approximation – which estimates $R_{rs}(\lambda)$ from $a(\lambda)$ and the backscattering coefficients $b_b(\lambda)$. The majority of IOP retrieval algorithms developed by the community have used the quasi single-scattering approximation (QSSA) originally introduced by Hansen (1971) and translated to ocean color by Gordon (1973) (see also Zege et al., 1991). This approach was refined further by Gordon (1986) who approximated the sub-surface remote reflectances $r_{rs}(\lambda)$ with a Taylor series expansion:

$$r_{rs}(\lambda) = \sum_{i=1}^N G_i u(\lambda)^i, \quad (1)$$

with

$$u(\lambda) \equiv \frac{b_b(\lambda)}{a(\lambda) + b_b(\lambda)}. \quad (2)$$

Most IOP retrieval algorithms have taken $N = 2$ and set the coefficients as constants $G_1 = 0.0949$ and $G_2 = 0.0794$, i.e. values independent of wavelength. In this manuscript and for the default mode of BING, we adopt the same prescription and coefficients, but scrutinize the accuracy of this assumption in Supp 6.2. For the results in the main text, we assume a perfect forward model, i.e. we use Equation 1 to generate the target $r_{rs}(\lambda)$ and perform the fits on these values. In practice, we work with remote-sensing reflectances $R_{rs}(\lambda)$ following a standard conversion from $r_{rs}(\lambda)$ (Lee et al., 2002):

$$r_{rs}(\lambda) = \frac{R_{rs}(\lambda)}{0.52 + 1.17R_{rs}(\lambda)} \quad (3)$$

For the development and testing of BING, we have leveraged a large set of $a(\lambda), b_b(\lambda)$ spectra made public by Loisel et al. (2023) (hereafter L23). We use their $X = 4, Y = 0$ model which includes inelastic scattering (not relevant here) and the Sun at the zenith. The IOP spectra were generated from their database of in-situ measurements of phytoplankton $a_{ph}(\lambda)$ and models of several additional constituents: CDOM $a_g(\lambda)$, pure seawater $a_w(\lambda)$, and detritus $a_d(\lambda)$. L23 then generated estimates of the backscattering coefficients $b_{b,nw}(\lambda)$ following standard assumptions based on in-situ and laboratory work (see Loisel et al., 2023, for additional details). These 3,320 $a(\lambda)$ and $b_b(\lambda)$ spectra define our dataset and range from 350-750 nm at $\delta\lambda = 5$ nm sampling.

Despite the approximation of Equation 1, it does capture a salient aspect of the physics: the functional dependence of $R_{rs}(\lambda)$ on $u(\lambda)$ and thereby the IOPs $a(\lambda)$ and $b_b(\lambda)$. However, this dependence is the “bad” aspect of IOP retrievals: because $u(\lambda)$ is a function of the ratio of $b_b(\lambda)/a(\lambda)$:

$$r_{rs}(\lambda) = \text{Func} \left(\frac{b_b}{a} \right) , \quad (4)$$

the radiative transfer solutions are physically degenerate in b_b/a . Put succinctly, any IOP solution that recovers a set of $R_{rs}(\lambda)$ observations can be replaced by an infinite set that preserves the b_b/a ratio. Therefore, the retrieval is only tractable if one implements strong constraints (known as priors in Bayesian analysis) on the functional forms of $a(\lambda)$ and $b_b(\lambda)$.

In the following section, we examine the consequences of this physical degeneracy on IOP retrievals. We describe several standard priors from previous work and describe their impacts on IOP retrieval. Section 6.3 of the Supplement provides full details on BING and our specific approach to perform the Bayesian inference. We have also implemented standard χ^2 minimization (Levenberg-Marquardt) as a fitting option to speed-up model development and portions of the analysis. For results in the main text, we assume constant signal-to-noise (S/N) for the $R_{rs}(\lambda)$ measurements unless otherwise specified.

Note that the Bayesian approach in BING involves using Bayes’ theorem to update the probability of a hypothesis based on prior knowledge and new data. When retrieving IOPs from $R_{rs}(\lambda)$, this approach explicitly incorporates all available prior information about the IOPs and their uncertainties into the model. By doing so, it allows for a more transparent and rigorous estimation process. The Bayesian framework considers the likelihood of the observed $R_{rs}(\lambda)$ given the IOPs and combines it with the prior probability distributions of the IOPs to obtain a posterior distribution. This posterior distribution provides a probabilistic solution to the inverse problem, highlighting the most likely values of the IOPs while quantifying the uncertainties, leading to more reliable and informed retrievals.

3 The Good: Water as a prior

The “good” aspect of IOP retrievals is the presence of water which introduces an ever-present and precisely known¹ constraint on the problem. The absorption $a_w(\lambda)$ and backscattering $b_{b,w}(\lambda)$ spectra of pure seawater impose priors on the model that serve to partially alleviate the physical degeneracy described in the previous section. First, $a_w(\lambda)$ and $b_{b,w}(\lambda)$ span the entire spectrum and therefore couple the otherwise independent $R_{rs}(\lambda)$ values. Second, to the extent that the shapes of a_w and $b_{b,w}$ are unique relative to other constituents this helps one avoid the b_b/a degeneracy. Third, the strong absorption of water at $\lambda > 500$ nm and the relatively high magnitude of $b_{b,w}(\lambda)$ at $\lambda < 450$ nm define regions where one may retrieve information on the non-water components.

On the last point, Figure 1 compares the absorption and backscattering coefficients of water against one example of non-water spectra $a_{nw}(\lambda)$, $b_{b,nw}(\lambda)$ from the L23 dataset. As emphasized in the Figure, at red wavelengths $a \approx a_w(\lambda)$ and $b_{b,w} \approx b_{b,nw}$ such that the observations may constrain $b_{b,nw}$. Similarly at $\lambda < 450$ nm, $b_b \approx b_{b,w}$ and $a_{nw}(\lambda) > a_w(\lambda)$ such that the observations constrain a_{nw} . These inferences from Figure 1, however, rely on the strong (but frequently satisfied) prior that $a_w(\lambda) > a_{nw}(\lambda)$ at $\lambda > 500$ nm and $b_{b,w}(\lambda) > b_{b,nw}(\lambda)$ at $\lambda < 450$ nm. If this is relaxed, e.g. if $a_{nw}(\lambda)$ and $b_{b,nw}(\lambda)$

¹ Except in the ultraviolet, $\lambda < 400$ nm, which is intentionally ignored in this manuscript; Mason et al. (2016).

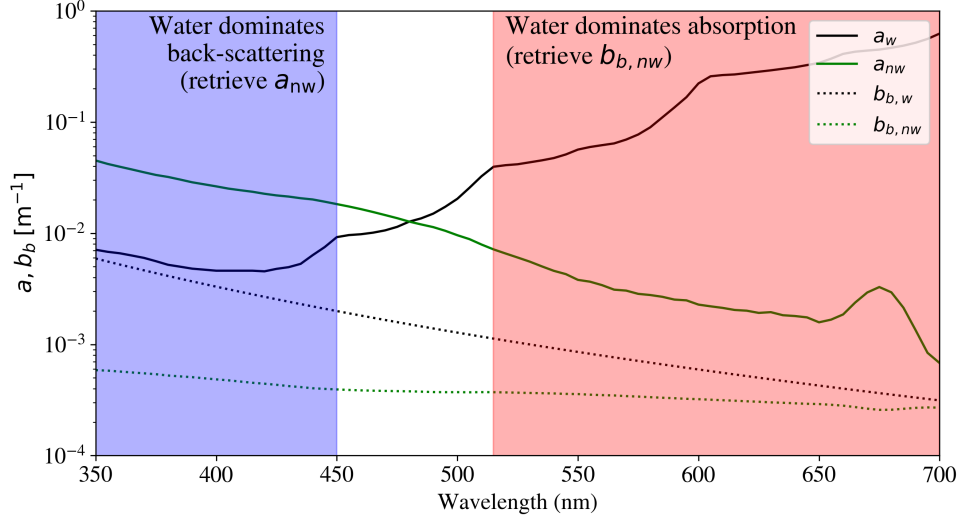


Figure 1. Comparison of the IOP spectra for water (a_w , $b_{b,w}$; black solid and dotted curves) against one example set of non-water spectra (a_{nw} , $b_{b,nw}$; green solid and dotted curves) from L23 (their index=170). The red region indicates where absorption by water dominates ($a_w > 5a_{nw}$). In this region, reflectance measurements constrain the non-water component of backscattering. Similarly, the blue region is where water dominates backscattering and retrievals may constrain a_{nw} . In turn, for observations with noise, the inversion problem has very limited constraints on the non-water components.

may take on *any* values then the b_b/a degeneracy forces an infinite set of solutions (i.e. no unique retrieval is possible; see Supp 6.4).

Stated another way, the greater the freedom that one allows for $a_{nw}(\lambda)$ or $b_{b,nw}(\lambda)$, the more degenerate the solutions. This fundamentally limits our ability to retrieve arbitrary $a(\lambda)$ or $b_b(\lambda)$ even in the presence of *perfect* data (infinite number of channels and no uncertainty). Therefore, no algorithm² can aim to retrieve arbitrary (Loisel & Stramski, 2000; Loisel et al., 2018) or even highly complex $a(\lambda)$ and $b_b(\lambda)$ (e.g. Chase et al., 2017). To make progress, one must also impose strong constraints on $a_{nw}(\lambda)$ and $b_{b,nw}(\lambda)$ to recover unique or most probable solutions. These priors, however, must insure that the values of a and b_b cannot vary at any individual wavelength where one seeks a retrieval in a way which holds their ratio constant.

4 The Ugly: Actual IOP retrievals

Let us now perform the “ugly”: attempted retrievals of $a_{nw}(\lambda)$ and $b_{b,nw}(\lambda)$ using assumed spectral shapes (priors) with a set of increasingly complex prescriptions. We follow common practice for models of $a_{nw}(\lambda)$ and $b_{b,nw}(\lambda)$ which have been informed by in-situ and laboratory measurements of ocean constituents. In turn, we will examine the maximum complexity that can be statistically constrained by observations designed to mimic satellite retrievals, e.g. data from multi-band and hyperspectral observations.

Consider first the simplest scenario we may conceive: a two-parameter [$k = 2$] model with both $a_{nw}(\lambda)$ and $b_{b,nw}(\lambda)$ taken as constant at all wavelengths:

² Including our own initial efforts with a more sophisticated algorithm than BING.

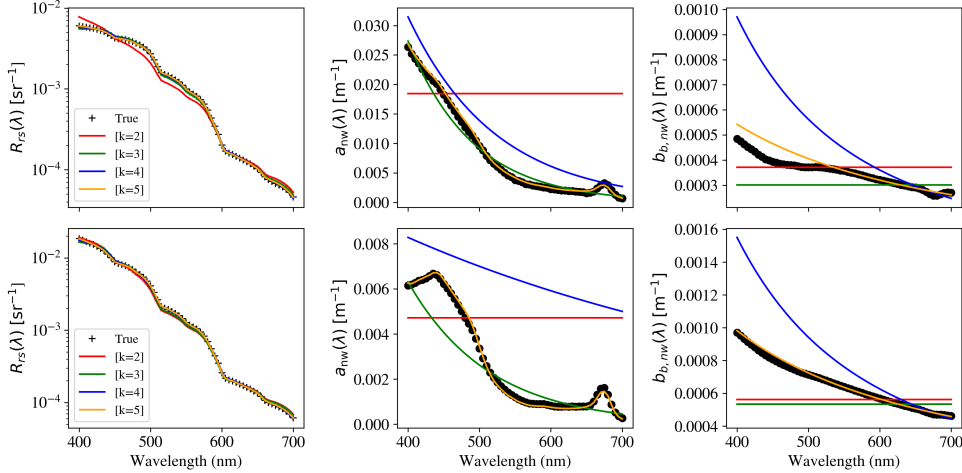


Figure 2. Retrievals of IOPs – (middle panels) $a_{nw}(\lambda)$ and (right panels) $b_{b,nw}(\lambda)$ from fits to (left panels) remote-sensing reflectances $R_{rs}(\lambda)$ assuming perfect radiative transfer and error-free data. The black points are the true values of $R_{rs}(\lambda)$, $a_{nw}(\lambda)$, and $b_{b,nw}(\lambda)$ for two examples from the L23 dataset: (index=170) which we chose as representative of the full dataset and (index=1032) which has $a_{ph} > a_{dg}$ at 440 nm. The figure shows solutions for a series of models with increasing complexity and number of free parameters k . These models are ($[k = 2]$; red) constant $a_{nw}(\lambda)$ and $b_{b,nw}(\lambda)$; ($[k = 3]$; green) constant $b_{b,nw}(\lambda)$ and a two-parameter exponential for $a_{nw}(\lambda)$; ($[k = 4]$; blue) exponential $a_{nw}(\lambda)$ and a power-law for $b_{b,nw}(\lambda)$; and ($[k = 5]$; orange) power-law $b_{b,nw}(\lambda)$ and $a_{nw}(\lambda)$ modeled by the exponential and a phytoplankton function (see text for further details). It is evident that all of the $k \geq 3$ models produce excellent fits to the $R_{rs}(\lambda)$ data at the several percent level.

$$a_{nw}(\lambda) = A_{cst} \quad (5)$$

$$b_{b,nw}(\lambda) = B_{nw} \quad (6)$$

We have fitted this model – including seawater absorption and backscattering – to two examples from the L23 dataset (Figure 2): one chosen to be representative of their full sample and the other chosen to have a higher than typical phytoplankton absorption $a_{ph}(\lambda)$ relative to the combined CDOM and detritus components $a_{dg}(\lambda)$ (i.e. $a_{ph}(440 \text{ nm}) > a_{dg}(440 \text{ nm})$). For these, we fit to $R_{rs}(\lambda)$ values calculated directly from Equation 1 and assume a constant S/N for the $R_{rs}(\lambda)$ values for the likelihood calculation³. Despite the extreme simplicity of this $[k = 2]$ model, the $R_{rs}(\lambda)$ fits are not too dissimilar from the true values, especially for the high $a_{ph}(\lambda)$ example⁴. This follows from our discussion of Figure 1: water backscattering and absorption dominates the solution at short and long wavelengths respectively and the non-water components have limited impact on the $R_{rs}(\lambda)$, i.e. we primarily measure seawater from IOP retrievals especially for ocean waters with low chlorophyll concentrations.

We consider three additional models of increasing complexity: the $[k = 3]$ model,

³ The best fits are identical for any constant S/N.

⁴ This a_{ph} -dominated spectrum has a low total non-water absorption, i.e. weak a_{dg} absorption.

$$a_{nw}(\lambda) = A_{exp} \exp[-S_{exp}(\lambda - 400)] \quad (7)$$

$$b_{b,nw}(\lambda) = B_{nw} \quad (8)$$

the $[k = 4]$ model,

$$a_{nw}(\lambda) = A_{exp} \exp[-S_{exp}(\lambda - 400)] \quad (9)$$

$$b_{b,nw}(\lambda) = B_{nw} (\lambda/600)^{\beta_{nw}} \quad (10)$$

and the $[k = 5]$ model,

$$a_{nw}(\lambda) = A_{exp} \exp[-S_{exp}(\lambda - 400)] + A_{ph} a_{ph}(\lambda) \quad (11)$$

$$b_{b,nw}(\lambda) = B_{nw} (\lambda/600)^{\beta_{nw}} \quad (12)$$

where λ is expressed in nm. A power-law is frequently adopted to describe $b_{b,nw}(\lambda)$, especially that related to particulate matter (Gordon & Morel, 1983). Here we allow β_{nw} to vary but consider fixed exponents in several models discussed in the Supplements. An exponential function, meanwhile, is commonly used to describe absorption by CDOM and/or detritus (Stramski et al., 2001). In-situ absorption measurements show typical values of $S_{exp} \approx 0.015$ for CDOM (Roesler et al., 1989) and $S_{exp} \approx 0.010$ for detritus (Stramski et al., 2001). Our fiducial models only require $S_{exp} > 0$ and we discuss stricter priors on that parameter below (and in Supp 6.6).

The $a_{ph}(\lambda)$ component in Equation 11 is introduced to capture “typical” absorption by phytoplankton. It is expected and observed that this component may exhibit the greatest complexity. Indeed, scientifically the community aims to distinguish the potentially large variations in phytoplankton families throughout the ocean and inland waters. Here, we adopt the parameterization of Bricaud et al. (1995):

$$a_{ph}(\lambda) = A_{ph}(\lambda) [Chla]^{E_{ph}(\lambda)} \quad (13)$$

with $Chla$ the Chlorophyll-a concentration in mg/m^3 and the tabulation of $A_{ph}(\lambda)$ and $E_{ph}(\lambda)$ are provided by Bricaud et al. (1998). We further set $Chla$ to the value used by L23,

$$Chla = a_{ph}(440 \text{ nm})/0.05582 \text{ m}^{-1} . \quad (14)$$

This last step is effectively another prior, but we will not penalize this model for the additional information in the analysis that follows.

Figure 2 shows the best solutions derived with BING for the $[k = 2 - 5]$ models. While the log-scaling of the $R_{rs}(\lambda)$ panels hides differences at the few percent level, it emphasizes that one requires nearly perfect observations to distinguish between the various models. The $[k = 3]$ model matches the data to within 10% at all wavelengths and the $[k = 4]$ and $[k = 5]$ models achieve several percent or less. As a result, the $[k = 4]$ model yields a reduced chi-squared $\chi^2_\nu \approx 1$ if we assume $\approx 5\%$ errors ($S/N=20$) in the $R_{rs}(\lambda)$ values. Visually, at least, Figure 2 emphasizes the (ugly) challenge of performing IOP retrievals: one is severely limited in the degree of unique information that can be derived.

We examine these points further in the Bayesian context by applying standard approaches for model selection, i.e., assessing the balance between model fit and complexity. Specifically, we have evaluated the Aikake and Bayesian information criteria (AIC,BIC) which are akin to χ^2 -difference tests (Bentler & Bonett, 1980):

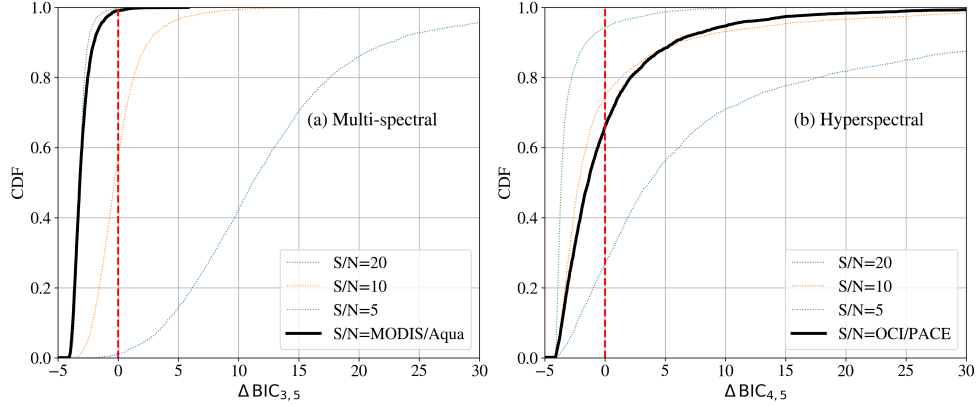


Figure 3. Evaluations of the difference in BIC values ΔBIC for fits to reflectance data derived from the 3,320 spectra of L23. The curves describe the cumulative distribution function (CDF) of the ΔBIC values. The left panel is for simulated MODIS observations (8 bands) with a series of signal-to-noise (S/N) assumptions (colored curves) and for retrievals adopting actual MODIS noise estimates from NASA validation Werdell & Bailey (2002). The $> 99\%$ negative $\Delta\text{BIC}_{3,5}$ values for the realistic noise case indicates the L23 spectra greatly favor models with only 3 parameters and without phytoplankton. [right panel] Similar analysis but for OCI/PACE-simulated observations with fixed S/N and for a best guess at nominal OCI/PACE performance (Supp 6.1). We find even with OCI that only $\approx 30\%$ of the L23 dataset favors the model with phytoplankton.

$$\text{AIC} = 2k - 2 \ln \mathcal{L} , \quad (15)$$

and

$$\text{BIC} = k \ln n - 2 \ln \mathcal{L} , \quad (16)$$

with n the number of $R_{rs}(\lambda)$ measurements and \mathcal{L} the likelihood function calculated assuming Gaussian statistics for uncertainties $\sigma = R_{rs}(\lambda)/(S/N)$. The likelihood function \mathcal{L} quantifies the probability of observing the data given the specific forward model and its parameters. Since it is calculated under the assumption of Gaussian (normal) statistics for the $R_{rs}(\lambda)$ uncertainties, this means that the observed data, i.e., the $R_{rs}(\lambda)$ measurements, are assumed to be normally distributed around the model predictions with the standard deviation. For our hyperspectral analysis where $n \gg 10$, the BIC offers a more stringent constraint but the results with AIC are qualitatively similar. A high AIC or BIC value implies that the model is less likely to be the best model given the data, considering both the fit and complexity. In the main text, we assess model selection by evaluating the difference in BIC for any two models $\Delta\text{BIC}_{i,j} = \text{BIC}_i - \text{BIC}_j$ where $\Delta\text{BIC}_{i,j} < 0$ indicates that model i is preferred and vice versa.

Figure 3 shows the ΔBIC values for simulated Moderate Resolution Imaging Spectroradiometer (MODIS) observations of the L23 spectra (see Supp 6.1 for details). The cumulative distribution function (CDF) on the y-axis represents the cumulative probability that the ΔBIC values for the 3,320 fits to the L23 $R_{rs}(\lambda)$ data are less than or equal to a specific value. Each ΔBIC value corresponds to a comparison between two models, specifically the BIC values for a model with and without phytoplankton parameters ($[k = 3]$ and $[k = 5]$ in the multi-spectral case, Figure 3a, and $[k = 4]$ and $[k = 5]$ in the hyper-spectral case, Figure 3b). If the CDF value is y_{CDF} at a specific ΔBIC value, it means that the $100 \times y_{\text{CDF}}\%$ of the ΔBIC values in the dataset are less than or equal to that specific value. Thus, the CDF curve shows the proportion of the dataset

for which the simpler model is preferred as a function of the ΔBIC value. The higher the CDF value at $\Delta\text{BIC} = 0$, the higher fraction of the dataset which favors the simpler model over the more complex one.

For the analysis with a realistic MODIS noise model, fewer than 1% of the spectra prefer the $[k = 5]$ model with phytoplankton. This holds true even though our analysis assumed a perfect forward model and perfect knowledge of the measurement uncertainties, without correlated errors. Allowing for these uncertainties would result in zero cases with $\Delta\text{BIC} < 0$. In fact, we find (Supp. Figure 9) that one cannot retrieve more than 3 parameters from MODIS observations and that even the $[k = 2]$ model is largely satisfactory. Without *perfect* knowledge of the absorption by CDOM one cannot retrieve phytoplankton from MODIS observations alone.

The curve corresponding to $S/N = 20$ in Figure 3a shows that while there is some support for the simpler model, indicated by the CDF values for positive ΔBIC , the more complex model, which includes additional parameters for phytoplankton, is generally preferred. This is because the CDF for negative ΔBIC values is low, indicating that the simpler model is not favored in most of the dataset. In other words, although the simpler model is supported in some cases, the overall trend indicates that the more complex model is usually favored for $S/N = 20$. Thus, reducing noise in the $R_{rs}(\lambda)$ data is essential when increasing model complexity. However, achieving $S/N = 20$ is challenging, even at blue wavelengths in open ocean Case 1 waters, as demonstrated in numerous validation studies (6.1). And, achieving $S/N = 20$ at $\lambda > 600$ nm where absorption by seawater alone is very high may be impossible (Zhang et al., 2022).

We reach even stronger conclusions for simulated SeaWiFS observations (Supp 6.1) which have fewer bands. Unless one identifies an approach to regularly achieve $S/N \gg 10$ measurements in the presence of all error terms (e.g. atmospheric corrections), phytoplankton cannot be retrieved from multi-spectral observations without strong, additional priors. In Supp 6.7, we examine the GIOP and GSM models which assume a fixed and steep S_{exp} shape parameter and the negative outcomes of this assumption.

Now consider an assessment using L23 spectra with simulated Ocean Color Instrument (OCI) hyperspectral observations on the Plankton, Aerosol, Cloud, ocean Ecosystem (PACE) satellite (see Supp 6.1 for details). Our fiducial case uses the L23 spectral sampling and we limit the observations to $400 \text{ nm} < \lambda < 700 \text{ nm}$, outside of which systematics of the L23 dataset and instrumentation dominate the uncertainties in $R_{rs}(\lambda)$, and poor knowledge of the wavelength dependence of the ocean’s constituents preclude confident analysis. Figure 3 shows the distribution in the difference in BIC values, ΔBIC , between the $[k = 4, 5]$ models assuming several choices for the S/N and our estimate for the OCI/PACE noise from v1.0, Level 2 products (Supp 6.1). We find that OCI/PACE may not recover an assemblage signature of phytoplankton from water with properties similar to those represented by the L23 dataset. We are led to conclude that one can may retrieve four parameters for IOPs from a OCI-like observation and possibly a fifth. Two of these numbers describe the amplitude and shape of $a_{nw}(\lambda)$ parameterized as an exponential and two numbers describe $b_{b,nw}(\lambda)$ modeled as a power-law. Absent strong priors that account for one of these four, extracting even one number describing $a_{ph}(\lambda)$ (at all wavelengths) will be challenging.

5 Conclusions and Future Prospects

In this manuscript, we have introduced BING, a Bayesian inference algorithm for IOP retrievals utilizing the Gordon coefficients for radiative transfer. We have reemphasized a known but under-appreciated physical degeneracy in the radiative transfer – $r_{rs}(\lambda)$ is a function of b_b/a which strictly limits one ability to retrieve $a(\lambda)$ and $b_b(\lambda)$ without strong priors. Two of the priors are natural: water both absorbs and scatters light with

precisely known coefficients, at least for wavelengths $\lambda > 400$ nm. We demonstrated, however, that even these constraints are insufficient; indeed, water frequently dominates the model limiting the extraction of additional information. Consequently, we found that multi-spectral observations with published uncertainties Zhang et al. (2022) cannot reliably retrieve phytoplankton, and that even hyperspectral observations (e.g. OCI/PACE) will be challenged (Figure 3).

While the ill-posed nature of the inversion problem to retrieve IOPs from $R_{rs}(\lambda)$ is a known issue, this study offers significant value by providing a comprehensive analysis and quantification of this degeneracy. The methodology rigorously examines the implications of spectral ambiguities on satellite-derived IOP products, highlighting the specific conditions and parameters where these ambiguities are most pronounced. This detailed investigation not only reinforces the necessity for caution in interpreting satellite products, but also advances the understanding of the limitations and potential improvements in current algorithms. By revealing the extent and impact of these ambiguities, the study contributes insights for the refinement of remote sensing techniques and the development of more accurate ocean color models. Consequently, this work is a crucial step forward in enhancing the precision and reliability of ocean color remote sensing.

Previously, Cael et al. (2023) reached a similar inference as one of our primary conclusions – the limited information content of remote-sensing observations. Specifically, they analyzed the degrees of freedom (DoF) of $R_{rs}(\lambda)$ data through a standard principal component analysis finding that in-situ $R_{rs}(\lambda)$ data with MODIS sampling has only 3 DoF and inferred only DoF=2 for remotely sensed $R_{rs}(\lambda)$. Our analysis, which includes several constraints, such as water absorption and scattering, yields at least one additional parameter but the overarching implication is similar: retrievals from $R_{rs}(\lambda)$ observations have limited information content.

On statistical grounds the community could not and cannot retrieve $a_{ph}(\lambda)$ from $R_{rs}(\lambda)$ provided one allows for exponential absorption by CDOM and/or detritus which are always present. In fact, this component (a_{dg}) tends to exceed a_{ph} , even in the open ocean (Siegel et al., 2013; Hooker et al., 2020). Previous work that published estimates of $a_{ph}(\lambda)$ required very strict priors on the shape of S_{exp} (Supp 6.6), leading to significant bias in estimates of a_{ph} . In the cases where S_{exp} was allowed to vary (Boss & Roesler, Chapter 5 Lee, 2006), the errors on a_{ph} were severe and limited retrievals only to upper limits on a_{ph} , consistent with this work.

Do our results therefore invalidate the past several decades of research and data products using satellite-based ocean color observations? At the least, all previous retrievals from $R_{rs}(\lambda)$ must be further scrutinized. We assert uncertainties and biases were frequently (possibly always) underestimated, and substantial correlations between retrieved parameters will be present. Unfortunately even relative analyses of $a_{ph}(\lambda)$ may be subject to large error. There are, however, key products that are primarily (and very nearly exclusively) empirical, i.e. generated without any radiative transfer model (Stramski et al., 2022). These empirically-based algorithms may circumvent the radiative transfer issues raised here, but as emphasized by Cael et al. (2023), one cannot retrieve an arbitrary number of such quantities from visible domain $R_{rs}(\lambda)$ observations. Therefore, the suite of products generated by the community to date are highly coupled and correlated. The limited information content of $R_{rs}(\lambda)$ measurements subject to realistic uncertainties is inherent to the problem.

While the results from Figure 3b indicate that hyperspectral observations offer a substantial improvement over multi-spectra data, even *detecting* phytoplankton remains challenging. We reemphasize that the results presented here have assumed a perfect forward model (i.e. no error in the radiative transfer calculation), uncorrelated uncertainties, a perfect model for water absorption and backscattering, and homogeneous seawater (no vertical or horizontal spatial variations). Furthermore, even if we surmount these

issues, we may only be able to extract a single parameter describing phytoplankton, e.g., the a_{ph} amplitude at $\lambda \approx 440$ nm. And, strictly speaking, this may be attributed to *any* absorption component (not solely a_{ph}) that does not follow the exponential described by CDOM and detritus.

How might we proceed? It is abundantly clear that we must identify the optimal way to parameterize the problem to make most effective use of the 4 or 5 parameters that describe $a_{\text{nw}}(\lambda)$ and $b_{b,\text{nw}}(\lambda)$. For example, if we know β_{nw} (i.e. fix its value as a prior), we would not “waste” a free-parameter to estimate its value. In short, we must harness our knowledge of the ocean from previous in-situ measurements (or current, if one can afford them) to set priors on the model. These priors should be geographically and temporally variable to reflect different oceanic conditions. Because strict and biased priors have been shown to lead to inaccurate and uncertain retrievals, one must proceed cautiously. Empirically derived priors can help mitigate these issues by providing a more accurate representation of the ocean’s optical properties.

One obvious community-wide effort would be to develop and agree upon strong priors for S_{exp} . This is current practice in many existing algorithms (e.g. GIOP, GSM, which set S_{exp} to a single value), but we describe the negative consequences of this extreme approach in Supp 6.6. Instead, we encourage the community to generate S_{exp} priors as probability distribution functions that vary with geographic location and time and then revisit these in our changing climate. Additionally, we must include more observations, both from space and in-situ. From space, we must leverage the *Chla* fluorescence signal at ≈ 685 nm (Wolanin et al., 2015) whose production and radiative transfer are distinct from that of IOP retrievals. From the ocean, in-situ observations provide invaluable validation data and may establish priors like those for S_{exp} . Non-visible in-situ optical observations have been shown to improve retrievals of CDOM absorption, and could be retained to better partition signals related to CDOM and phytoplankton biomass. Constraints on β_{nw} , as a function of location and season, and physical priors on the coupling of $a(\lambda)$ to $b_b(\lambda)$ for individual components from the physics of absorption and scattering could be impactful.

Developing community-wide Bayesian retrieval algorithms is also recommended. The ocean color remote-sensing community should be encouraged to adopt a Bayesian framework for IOP retrievals such as BING, explicitly including all priors and their uncertainties. A Bayesian approach allows for a more transparent and rigorous incorporation of prior knowledge and uncertainties, leading to more reliable retrievals. Unlike BING, however, Bayesian algorithms must adopt an accurate forward model and its uncertainties, include correlated and systematic error in the observations, and harness new data sources. We have initiated such a project – Intensities to Hydrolight Optical Properties (IHOP) – and encourage community adoption and development. The scientists focused on atmospheric corrections have already embarked on this journey following the original insight of Frouin & Pelletier (2015). Ultimately, we should consider merging the two, i.e., generate an end-to-end Bayesian model that fits top-of-atmosphere radiances to retrieve IOPs.

Increasing the spectral resolution of satellite observations can provide more detailed information about the absorption and backscattering properties of phytoplankton, thereby reducing the impact of degeneracies. Thus, the development and deployment of hyperspectral satellites with high spectral resolution across the visible and near-infrared spectrum are recommended. The recently launched PACE satellite will lead the way. Additionally, exploring alternative remote-sensing techniques, such as Lidar and fluorescence-based methods, and incorporating polarization information to complement traditional ocean color observations, should be considered. These advanced techniques may provide independent measurements that help resolve ambiguities and improve the overall accuracy of phytoplankton estimates, although information gained using these new techniques should be clearly demonstrated and defined first in the field.

Table 1. MODIS Data

Band (nm)	$\sigma(R_{rs}(\lambda))$ (sr ⁻¹)
412	0.0012
443	0.0009
488	0.0008
531	0.0007
547	0.0007
555	0.0007
667	0.0002
678	0.0001

Notes: The error has assumed that 1/2 of the variance is due to the in the in-situ measurements.

Addressing the uncertainty in atmospheric corrections is another critical recommendation. Improving atmospheric correction algorithms to reduce the uncertainties they introduce into ocean color retrievals is crucial. Incorporating advanced atmospheric models and ancillary data (e.g., aerosol properties) can enhance correction accuracy. Atmospheric corrections are a significant source of error in remote-sensing reflectance measurements, and reducing these uncertainties is essential for accurate phytoplankton IOP retrievals. Continued implementation of dark-pixel correction schemes, for example, removes non-visible information and is inconsistent with in-situ observations of the aquatic light field.

Promoting interdisciplinary collaboration is also essential. Fostering collaboration between oceanographers, remote-sensing experts, and radiative transfer modelers to address the complex challenges of IOP retrievals can bring together diverse expertise and perspectives, leading to more innovative and effective solutions. These should include individuals with mastery of statistics who can rigorously assess uncertainty and help develop robust and transparent algorithms.

By implementing these recommendations, the remote-sensing community can significantly enhance the accuracy and reliability of phytoplankton IOP retrievals, leading to better-informed biogeochemical models and ecological assessments. This comprehensive approach will help ensure that remote-sensing data accurately reflect the true state of the ocean’s biological and chemical processes, thereby supporting more effective environmental monitoring and management efforts.

6 Supplementary Materials

6.1 Data and their Uncertainties

As described in the main text, all of the absorption and scattering spectra examined in this manuscript were taken from Loisel et al. (2023) (aka, L23). Their dataset includes total absorption and scattering as well as the contributions from individual components (e.g. a_{ph} , a_d , a_g). The dataset also includes outputs from Hydrolight calculations (C. D. Mobley & Sundman, 2013) using these spectra as input, e.g. $R_{rs}(\lambda)$ and depth-resolved quantities like the diffuse absorption coefficient $K_d(\lambda)$. Specifically we use the L23 dataset with inelastic scattering and at 0 deg. solar and viewing zenith angle.

For many of the analyses presented here, we have independently generated simulated $R_{rs}(\lambda)$ spectra for several multi-spectral and hyperspectral missions. For the fits presented in this manuscript, we ignore the $R_{rs}(\lambda)$ provided by L23 and instead use Equa-

Table 2. SeaWiFS Data

Band (nm)	$\sigma(R_{rs}(\lambda))$ (sr^{-1})
412	0.0014
443	0.0011
490	0.0009
510	0.0006
555	0.0007
670	0.0003

Notes: The error has assumed that 1/2 of the variance is due to the in the in-situ measurements.

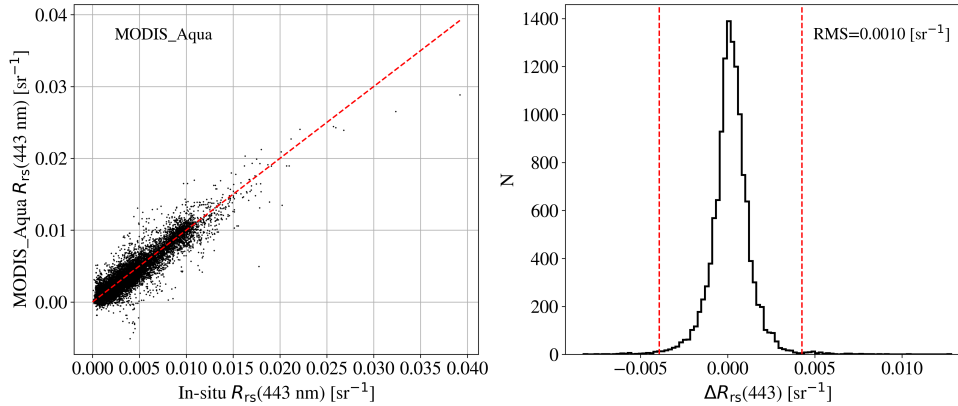


Figure 4. (left) Comparison of the MODIS measurements of $R_{rs}(\lambda)$ at $\lambda = 443 \text{ nm}$ against in-situ observations at the same wavelength. These were taken from the SeaBASS site (Werdell & Bailey, 2002) dedicated to MODIS matchups (SeaBASS, 2024). The points follow the over-plotted one-to-one line relatively well, albeit with significant scatter which we assess as the RMS noise in the MODIS observations. (right) Distribution of the difference between in-situ and satellite $\Delta R_{rs}(\lambda) = R_{rs}(\lambda)^{\text{in-situ}} - R_{rs}(\lambda)^{\text{MODIS}}$. The red dashed-lines show the 4σ interval beyond which we clipped the data when calculating the noise estimate (RMS).

tions 1-3 to calculate $R_{rs}(\lambda)$ from $a(\lambda)$ and $b_b(\lambda)$. We then resample these spectra to the bands/channels of several satellite missions:

MODIS/Aqua: We adopt 8 multi-spectral bands as listed in Table 1 corresponding to the MODIS Aqua mission and we evaluate $R_{rs}(\lambda)$ at the center of each. For uncertainties, we have estimated the RMS difference between satellite and in-situ $R_{rs}(\lambda)$ “match-up” measurements collated on the SeaBASS database (Werdell & Bailey, 2002) after iteratively clipping any 4σ outliers. Figure 4 shows an example of the data and clipping for one band. We further assumed that one half of the variance is due to the in-situ observations themselves. These RMS values are also provided in Table 1, and we find they are in good agreement with other estimations (Zhang et al., 2022; Kudela et al., 2019).

SeaWiFS/SeaStar: We followed a similar procedure for the Sea-viewing Wide Field-of-view Sensor (SeaWiFS) using 6 bands and the uncertainties provided in Table 2.

OCI/PACE: For simulated OCI/PACE spectra, we assumed $\delta = 5 \text{ nm}$ sampling and limited the wavelength range from 400–700 nm. The lower bound is due to (i) greater

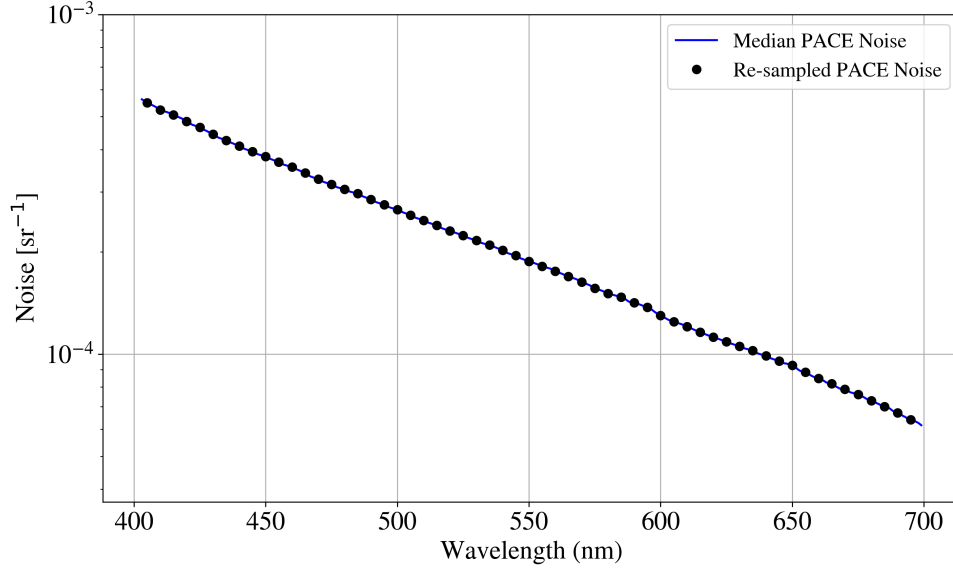


Figure 5. The blue curve is the median PACE uncertainty in $R_{rs}(\lambda)$ estimated in the Level 2 product, v1.0 for one granule (PACE_OCI.20240413T175656.L2.OC_AOP.V1_0_0.NRT.nc). The black dots are the values of $\sigma(R_{rs}(\lambda))$ adopted in this manuscript when simulating PACE spectra with noise.

uncertainties in the atmospheric corrections, (ii) greater uncertainty in water absorption and scattering, (iii) greater uncertainty in how best to parameterize the non-water components in the UV. The upper wavelength bound is to avoid systematics that likely dominate the uncertainty at the lowest $R_{rs}(\lambda)$ signals.

For the PACE noise model, we downloaded a single granule (2,175,120 pixels) of Level 2 data, v1.0: PACE_OCI.20240413T175656.L2.OC_AOP.V1_0_0.NRT.nc. We then took the median uncertainty spectrum (Rrs_unc Zhang et al., 2022) for all non-flagged data between 33-40N and 73-78W. This median spectrum is plotted in Figure 5 at the Level 2 wavelength sampling (≈ 2.5 nm). We also show the values adopted at our $\delta = 5$ nm sampling, and one notes that we did not adjust $\sigma(R_{rs}(\lambda))$ despite the larger sampling size. This is because OCI is over-sampled at $\delta = 2.5$ nm, i.e. the data is highly correlated. Further work should assess the degree of this correlation to obtain a better noise estimate. If we were to assume no correlation (i.e. reduce $\sigma(R_{rs}(\lambda))$ by $1/\sqrt{2}$), the results in Figure 3b would yield a higher fraction of spectra preferring 5 parameters: instead of $\approx 70\%$ of the L23 dataset showing $\Delta\text{BIC} < 0$, we find $\approx 30\%$ fail the criterion.

6.2 Taylor expansion model re-examined

To examine the use of Equation 1 as an approximation of the radiative transfer, consider Figure 6 which plots the Hydrolight-derived $R_{rs}(\lambda)$ of L23 converted to $r_{rs}(\lambda)$ with Equation 1 against the evaluated $u(\lambda)$ values using Equation 2 at 4 distinct wavelengths. These evaluations approximately follow a quadratic with zero y-intercept. Over-plotted with a dashed line is the Gordon approximation using the standard G_1, G_2 coefficients and Equation 1. Qualitatively, the Hydrolight outputs follow the relation yet lie systematically above the curve. At its extreme, the Taylor series approximation is off-set by $\approx 10\%$ at $\lambda = 370$ nm and $u(\lambda) = 0.35$.

To further illustrate the difference, we have fitted G_1, G_2 coefficients to the data at select wavelengths and recover similar G_1 values but G_2 values that vary significantly with wavelength ($G_2 \approx 0.07$ at $\lambda = 370$ nm, $G_2 \approx -1.2$ at $\lambda = 600$ nm). We also find that there is significant scatter around each of the fits with a relative RMS of $\approx 5\%$ at shorter wavelengths and 20% at the reddest wavelengths. We expect this scatter is inherent to Equation 1 and would be unavoidable if one uses this approximation even with wavelength-dependent coefficients. An accurate retrieval algorithm would need to account for these variations or otherwise suffer significant systematic error. This is the focus of a separate algorithm we are developing (IHOP), and we also refer the readers to recent advances in approximations of the radiative transfer equation (Twardowski et al., 2018).

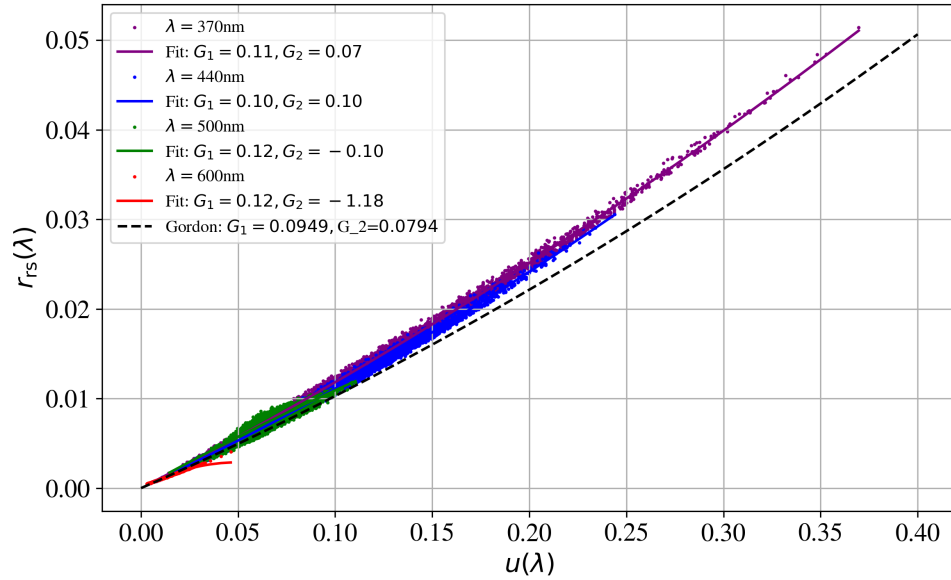


Figure 6. Sub-surface reflectances $r_{rs}(\lambda)$ generated with the Hydrolight radiative transfer code by L23 (converted from $R_{rs}(\lambda)$ using Equation 3) against $u(\lambda)$ as defined by Equation 2. The black dashed line shows the second order Taylor expansion of $r_{rs}(\lambda)$ in $u(\lambda)$ (Equation 1) with the Gordon coefficients most widely adopted by the community. In general, this curve underpredicts $r_{rs}(\lambda)$ as calculated with Hydrolight with a maximum offset of $\approx 10\%$ at $u(\lambda) = 0.35$ and $\lambda = 370$ nm. We also show a series of individual fits of Equation 1 to the data with the legend indicating the derived G_1, G_2 coefficients. Note that G_1 is largely independent of wavelength but that G_2 is strongly wavelength dependent (and anti-correlated).

6.3 Bayesian Inference

Provided the forward model and a parameterization of $a(\lambda)$ and $b_b(\lambda)$, the Bayesian inference is straightforward and a wealth of well-trodden approaches and software packages are available. For BING, we adopt the Monte Carlo Markov Chain (MCMC) formalism which empirically derives the posterior probabilities for the $a(\lambda), b_b(\lambda)$ parameterization $P(X|Y)$ including full uncertainties and all of the cross-correlation terms. This requires the definition of a likelihood function $P(Y|X)$, which will have the form:

$$P(Y|X) \propto \exp \left\{ -\frac{1}{2} [Y - H(X)]^T C [Y - H(X)] \right\} \quad (17)$$

where Y represents the measured $R_{rs}(\lambda)$ values, C is the full covariance matrix of $R_{rs}(\lambda)$ including correlations, and $H(X)$ is the forward model of $R_{rs}(\lambda)$ at the locations of Y .

It can be shown that an MCMC analysis converges to the exact solution if run for an infinitely long time; in practice, the calculations tend to converge after $\approx 10,000$ iterations. For the analysis here, we generally run for 75,000 trials with at least 2 walkers per parameter (and at least 16 walkers) and only analyze the last 7,000 iterations of each. This release of BING uses the EMCEE sampler (Foreman-Mackey et al., 2013) which was developed for astrophysical applications and has seen wide-spread adoption in the field (over 8,000 citations).

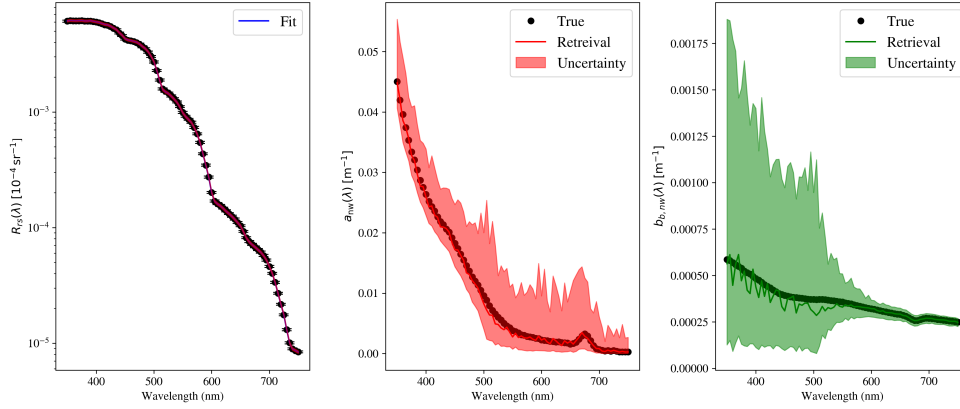


Figure 7. Example of a BING retrieval of $a_{nw}(\lambda)$ (center) and $b_{b,nw}(\lambda)$ (right) from the $R_{rs}(\lambda)$ spectrum (left). In this example, we parameterized $a_{nw}(\lambda)$ and $b_{b,nw}(\lambda)$ with 81 free parameters, one for every wavelength channel. Owing to the physical degeneracy in the radiative transfer equation, $R_{rs}(\lambda) = F(a/b_b)$, there are an infinite number of solutions yielding an infinite uncertainty in $a_{nw}(\lambda)$ and $b_{b,nw}(\lambda)$. Here, the Bayesian inference was only performed for 70,000 steps and has not fully described the (infinite) posterior space (and never would).

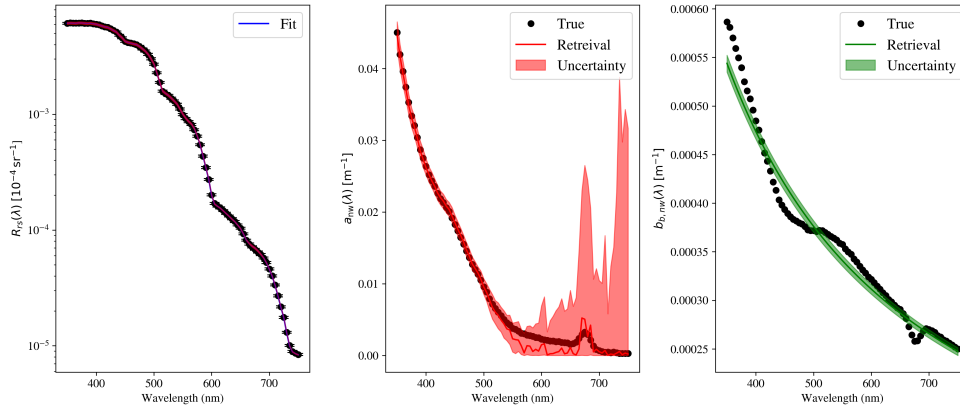


Figure 8. Same as Figure 7 but with $b_{b,nw}(\lambda)$ parameterized as a power-law with fixed exponent and $a_{nw}(\lambda)$ still allowed to have any shape. Again, there are an infinite number of solutions, only partially captured by the 75,000 steps of the sample.

6.4 Fits with $a(\lambda)$ and/or $b_b(\lambda)$ free to vary

One point emphasized in this manuscript is that one cannot retrieve arbitrary $a(\lambda)$ or $b_b(\lambda)$ or even $a_{nw}(\lambda)$ and $b_{b,nw}(\lambda)$ because of a physical degeneracy in the inversion of the radiative transfer equation (Equation 4). To demonstrate this with two examples, we performed an IOP retrieval of $a_{nw}(\lambda)$ and $b_{b,nw}(\lambda)$ assuming a perfect forward model (Equation 1), perfect knowledge of the uncertainties, and perfect knowledge of water ($a_w, b_{b,w}$). In this case, we solve for “arbitrary” $a_{nw}(\lambda)$ and $b_{b,nw}(\lambda)$ by parameterizing each with 81 free parameters, one per wavelength channel. We show the fits to $R_{rs}(\lambda)$ for the index=170 spectra of L23 in Figure 7 and the retrievals with 95% confidence intervals, finding that our solutions for $a_{nw}(\lambda)$ and $b_{b,nw}(\lambda)$ start “blowing up” after only 50,000 samples.

To further emphasize the point, we refit the data but constrained $b_{b,nw}(\lambda)$ to be a power-law with a fixed exponent β_{nw} set at a value that closely corresponds to the known $b_{b,nw}(\lambda)$ spectrum and only allow the amplitude B_{nw} of $b_{b,nw}(\lambda)$ to vary in the retrieval. Once again, the solution diverges (Figure 8) although more slowly. If we were to run for infinite samplings, we would recover an infinite uncertainty. With an arbitrary $a_{nw}(\lambda)$ spectrum, we can match any change to the amplitude of $b_{b,nw}(\lambda)$ and maintain constant a/b_b . Therefore, even with the strong constraint of water and just a single degree of freedom for $b_{b,nw}(\lambda)$, we still cannot retrieve arbitrary $a_{nw}(\lambda)$. This physical degeneracy limits the information content of retrievals and precludes arbitrary functional forms for $a_{nw}(\lambda)$ and $b_{b,nw}(\lambda)$, e.g. models which strive to retrieve arbitrary $a_{nw}(\lambda)$ are ruled out.

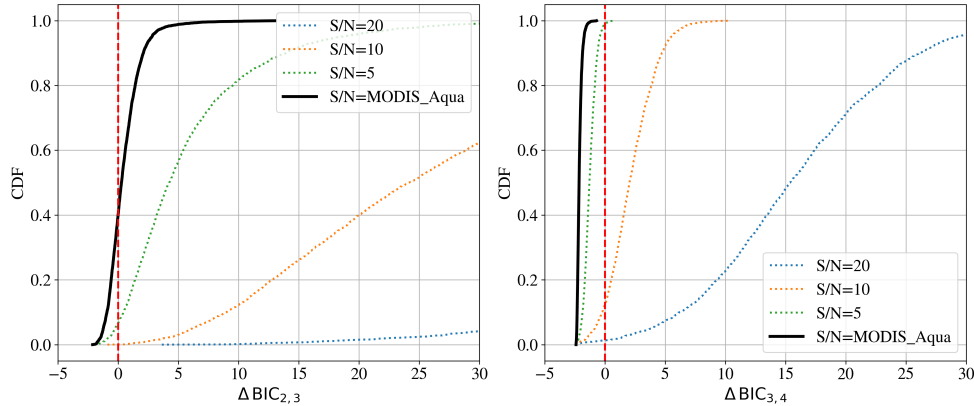


Figure 9. Additional BIC analyses on simulated MODIS spectra. The (left) panel compares the $[k = 2]$ and $[k = 3]$ models where we find that only $\approx 50\%$ of the L23 dataset favors anything more complex than the two-parameter, constant model. The (right) panel demonstrates that the $[k = 4]$ model is disfavored for the entire L23 dataset.

6.5 Additional BIC Analysis

We have compared additional pairs of models for the simulated multi-spectral $R_{rs}(\lambda)$ spectra than those in the main text. These additional analyses explore further the conclusion that such datasets are limited to retrieving a total of $k=3$ parameters describing $a_{nw}(\lambda)$ and $b_{b,nw}(\lambda)$ from multi-spectral, satellite observations.

Figure 9 shows ΔBIC distributions for the $[k = 2]$ vs. $[k = 3]$ model and the $[k = 3]$ vs. $[k = 4]$ model. Remarkably, we find that approximately half of the L23 dataset is optimally described by the constant IOP model. The results in Figure 9 show clearly

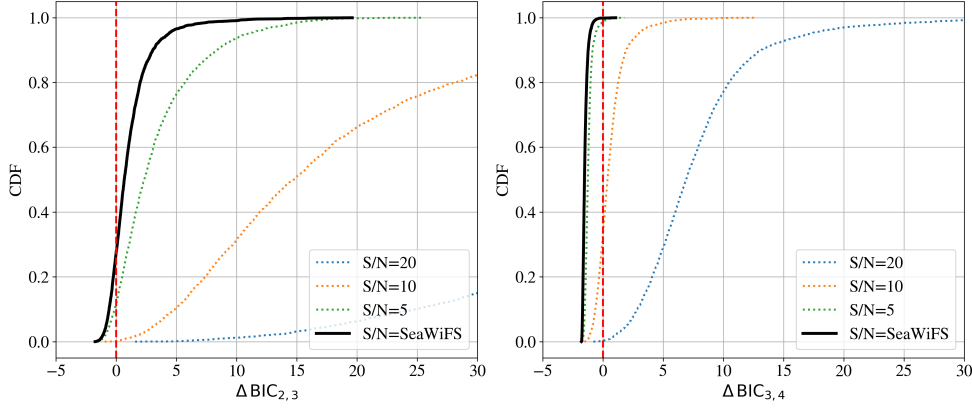


Figure 10. BIC analysis of simulated SeaWiFS spectra for (left) the $[k = 2]$ vs. $[k = 3]$ models and (right) $[k = 3]$ vs. $[k = 4]$. Approximately 30% of the L23 dataset favors the $[k = 2]$ model and only a few favor the $[k = 4]$ model. Similar to MODIS, multi-spectra observations generally prefer a model with $k < 3$ parameters.

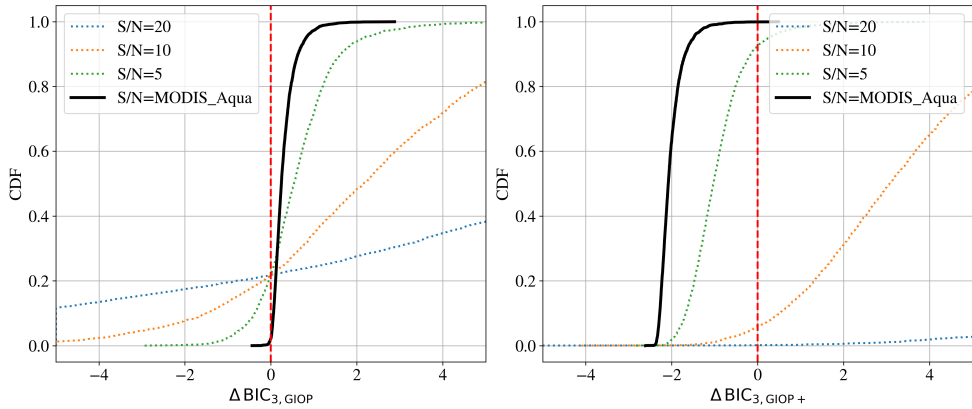


Figure 11. These panels describe the BIC analysis assuming MODIS-like observations for two models designed to match standard GIOP configurations. The (left) panel compares our $[k = 3]$ model against the standard $k=3$ parameter configuration of GIOP (see text for full details). We find this GIOP model is preferred, which we speculate is due to the extra freedom to fit the $R_{rs}(\lambda)$ at blue wavelengths where the S/N in MODIS is highest. (right) Results for the GIOP+ model ($k=4$ parameters) which lets β_{nw} be an additional free parameter. This model is disfavored for the entire dataset, further evidence that one cannot recover 4 parameters from MODIS observations.

that the $[k = 4]$ model is disfavored for *all* of the L23 dataset. This latter result greatly supports the conclusion on multi-spectral data given in the main text. Not surprisingly, the conclusions are even stronger for SeaWiFS spectra (Figure 10).

Now consider Figure 11 which presents ΔBIC distributions for two ‘‘GIOP’’ models which assume an exponential component for $a_{nw}(\lambda)$ with fixed shape parameter $S_{exp}=0.018\text{nm}^{-1}$, the Bricaud formulation for $a_{ph}(\lambda)$ and either (i) GIOP: the Lee et al. (2002) approach to estimating the power-law exponent of $b_{b,nw}(\lambda)$ or (ii) GIOP+: allowing β_{nw} to be free.

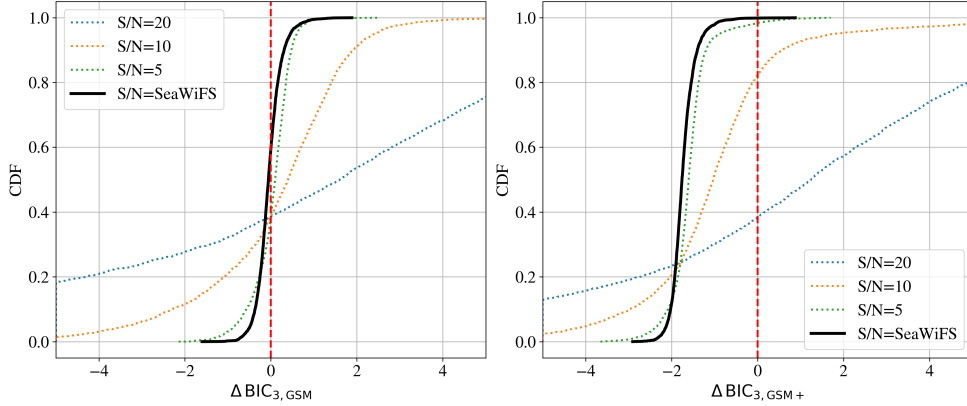


Figure 12. Similar to Figure 11 but for GSM models and using simulated SeaWiFS spectra. As with the GIOP models, we find the GSM model is favored over our $[k = 3]$ model but that a $k=4$ parameter version – GSM+ which lets β_{nw} be free – is highly disfavored.

This means $k=3$ free-parameters for GIOP⁵ – A_{exp} , A_{ph} , and B_{nw} – and a $k=4$ for GIOP+ (β_{nw}). Figure 11 shows that this model is favored over our fiducial $[k = 3]$ model which has no phytoplankton but free S_{exp} . This implies that strong priors on S_{exp} can lead to the inference of additional absorption (e.g. phytoplankton). We show below, however, the negative consequences of this overly strict prior, especially adopting a steeper slope than that typically found in the ocean. The figure also demonstrates that another parameter (GIOP+) cannot be extracted from the data.

Figure 12 shows ΔBIC distributions for two “GSM” models which also have a fixed exponential but with an even steeper slope ($S_{exp}=0.0206\text{nm}^{-1}$) and a power-law for $b_{b,nw}(\lambda)$ with fixed exponent $\beta_{nw}=1.0337$ (GSM) or letting β_{nw} be free (GSM+). Therefore, these are also $k=3$ and $k=4$ models with the same parameters as GIOP and GIOP+. We find that this mode is favored over the $[k = 3]$ model for only 33% of the L23 dataset. Similar to the GIOP model, we show in Supp 6.6 that its $a_{ph}(\lambda)$ retrievals are both highly biased and uncertain.

6.6 Treatment of S_{exp}

The previous section introduced the GSM and GIOP models which adopt fixed S_{exp} shape parameters for the exponential term in $a_{nw}(\lambda)$. We now examine that choice in the context of the L23 dataset and then consider the consequences for $a_{ph}(\lambda)$ retrievals in the following sub-section.

For our fiducial treatment of the exponential component in $a_{nw}(\lambda)$ (Equation 7), the only constraint placed on the shape parameter S_{exp} was that it be positive-definite ($S_{exp} > 0 \text{ nm}^{-1}$). Let us scrutinize that prior as it affects the potential to retrieve phytoplankton and any other constituents (see the previous section). Figure 13 shows the S_{exp} values derived with the $[k = 4]$ model (no phytoplankton) against the fraction of non-water absorption associated with phytoplankton at 440 nm in the L23 spectra, a_{ph}/a_{nw} . The two quantities are anti-correlated because the increased presence of phytoplankton relative to CDOM and detritus tends to give a shallower, non-water absorption spectrum.

⁵ Although we note that the shape of $a_{ph}(\lambda)$ and $b_{b,nw}(\lambda)$ are informed by the data such that it may be considered to have greater than $k=3$.

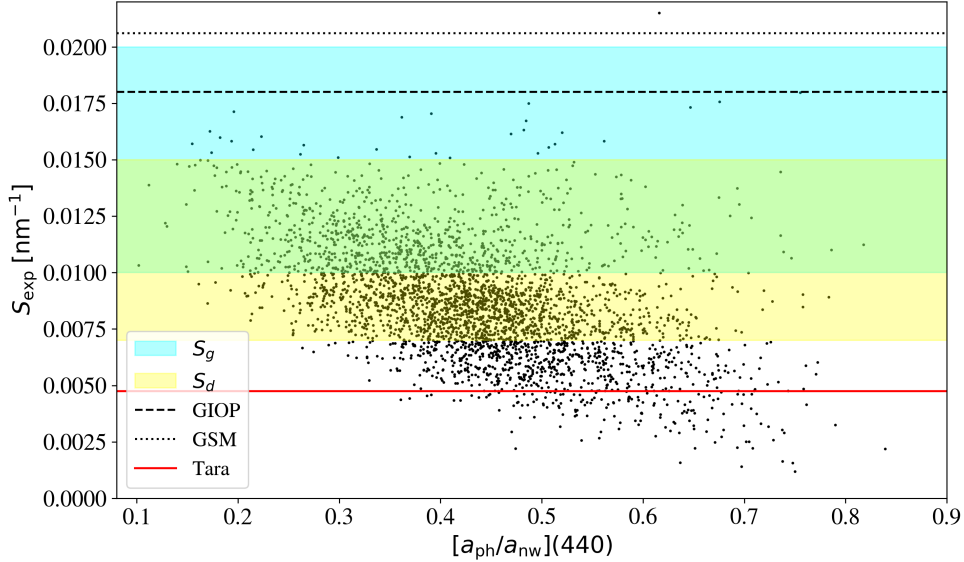


Figure 13. The dots plot the best fit shape parameter S_{exp} for the L23 spectra using the $[k = 4]$ model (no phytoplankton component) versus the amplitude of a_{ph} to a_{nw} at 440 nm. The two are correlated, albeit with large scatter. The blue and yellow shaded regions indicate the ranges of exponential shapes for CDOM and detritus (S_g, S_d) respectively adopted by L23. Not surprisingly, the majority of retrieved S_{exp} lie within these loci. The ones with shallower slope, however, may be attributed to the presence of phytoplankton which effectively flattens $a_{nw}(\lambda)$ at $\lambda \approx 450$ nm. The black dotted/dashed lines demarcate the fixed values of S_{exp} assumed by the GIOP/GSM algorithms for $a_{dg}(\lambda)$. These are steeper values than the typical S_g (and all S_d) values adopted by L23. In addition, we shows the S_{exp} derived from an extreme, CDOM-subtracted *Tara* absorption spectrum collected off the coast of Africa (see Prochaska & Gray, 2024) which demonstrates at least one instance of a very low S_{exp} in the ocean.

We find, as anticipated, that the majority of retrieved S_{exp} values lie within the loci of shape parameters assumed by L23 for CDOM and detritus based on (Lee, 2006). There is, however, a non-negligible set of retrieved S_{exp} values that are lower than the lowest value assumed by L23; these are partially due to strong phytoplankton absorption. If one were to adopt a stricter prior on S_{exp} than $S_{exp} > 0 \text{ nm}^{-1}$, therefore, one may find statistical evidence for phytoplankton absorption (formally, a distinct component from the best-fit exponential). Indeed, we found this to be the case for the GIOP and GSM models (Figures 11,12) although it is now apparent from Figure 13 that their choices for S_{exp} lie at the upper end of S_{exp} values measured in the ocean (GIOP) or even beyond (GSM). This was by intentional for GSM (Maritorena & Siegel, 2005), as its designers derived fixed values for S_{exp} and β_{nw} by achieving best retrievals when compared against in-situ data. However, their treatment of errors may not have been well suited to actual SeaWiFS uncertainties (Table 2) and we show below that the model is both biased and yields highly uncertain $a_{ph}(\lambda)$ estimates (in fact, primarily upper limits).

6.7 $a_{ph}(\lambda)$ Retrievals from GSM and GIOP

While the results in Figure 11 and 12 lend support that the GSM and GIOP models as designed may yield a positive detection of $a_{ph}(\lambda)$, it is important to appreciate the limitations. Consider first individual fits. Figures 14 and 15 show BING analyses on a

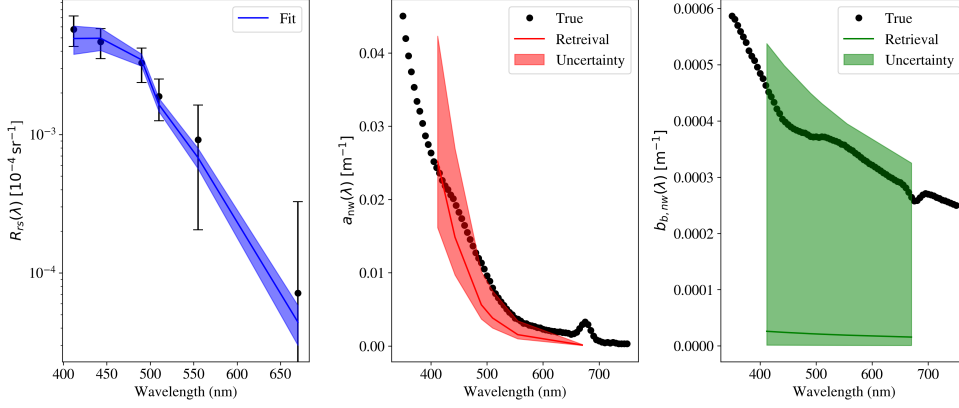


Figure 14. BING inferences from the (left) $R_{rs}(\lambda)$ spectra for (center) $a_{nw}(\lambda)$ and (right) $b_{b,nw}(\lambda)$. These results are for a fit to the index=170 spectrum of L23 assuming MODIS observations and the GIOP model. Note that we have not perturbed the data by the estimated MODIS noise but instead evaluate at their actual values. The shaded regions show 90% confidence intervals from the posterior draws. Clearly, the $b_{b,nw}(\lambda)$ and $a_{nw}(\lambda)$ estimations are highly uncertain.

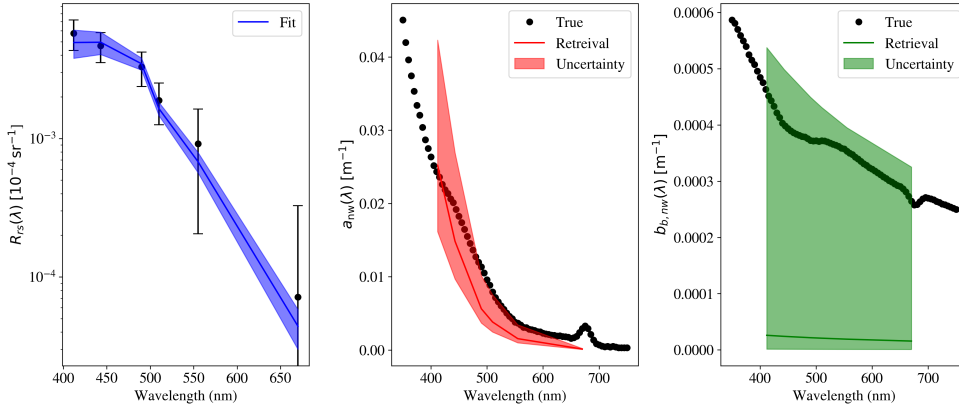


Figure 15. Same as Figure 14 but for GSM fitted to simulated SeaWiFS $R_{rs}(\lambda)$ spectra.

representative spectrum from L23 (index=170) for GIOP with MODIS observations and GSM on SeaWiFS. It is evident that the algorithm yields only an upper limit in B_{nw} and that the estimates of A_{exp} and A_{ph} are highly uncertain. One notes the large uncertainties and the (weak) degeneracies between the parameters. Therefore, while one retrieves a non-zero, best-estimate for $a_{ph}(\lambda)$, $A_{ph}=10^{-4} \text{ nm}^{-1}$ is contained within the 90% confidence interval.

We then performed a new set of inferences on the entire L23 dataset assuming MODIS and SeaWiFS simulated spectra for the GIOP and GSM models respectively. In both cases, we calculated $R_{rs}(\lambda)$ from Equations 1 and 3 and performed the inversion with the same model and without perturbing the $R_{rs}(\lambda)$ values due to the presence of noise. The retrievals are presented in Figures 16 and 17. In the second, more realistic case, we perturbed the $R_{rs}(\lambda)$ by the noise model for each satellite (Tables 2, 1), and present these in Figures 18 and 19. Clearly, the retrievals of a_{ph} and $b_{b,nw}$ are highly uncertain at all values, with nearly two orders of magnitude of scatter. Therefore, the detection of $a_{ph}(\lambda)$, if it were possible with multi-spectral observations, would be highly uncertain.

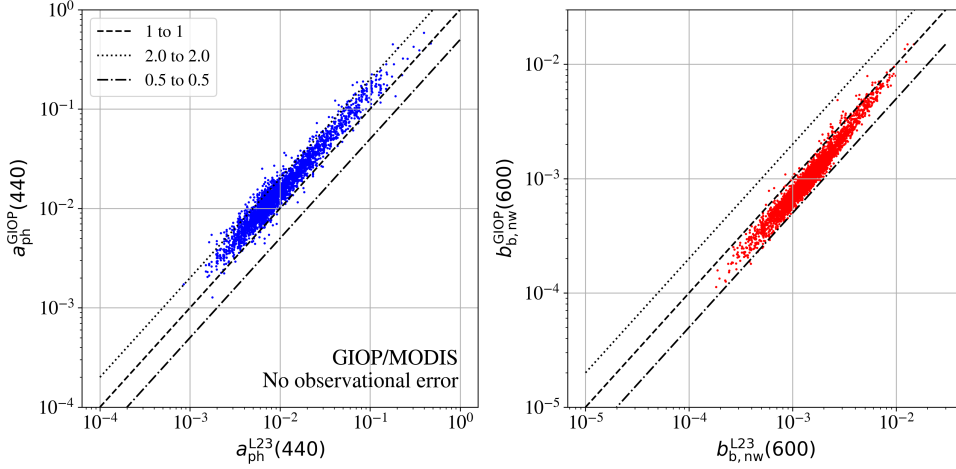


Figure 16. Comparison of retrieved phytoplankton absorption (left) and particulate backscattering (right) from GIOP on simulated MODIS spectra against the known values of the L23 dataset. These are for a perfect forward model and zero error. It is evident that the $a_{ph}(\lambda)$ values are biased high, by approximately 50%. Similarly the $b_{b,nw}(\lambda)$ values from GIOP (at 600 nm) are low by 50% at small values and $\sim 20\%$ at larger values.

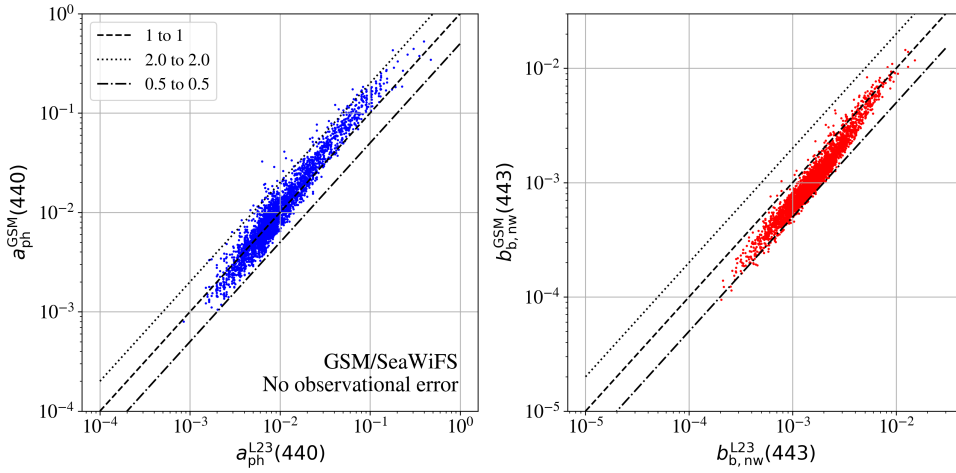


Figure 17. Same as Figure 16 but for the GSM model and simulated SeaWiFS spectra. As for GIOP, we find significant biases in the retrievals of several to many tens of percent.

The constraints inherent in inversion algorithms like GSM and GIOP do affect the confidence in interpreting changes in maps of retrieved variables such as chlorophyll concentration, absorption coefficients, and backscattering coefficients. The spectral ambiguity in $R_{rs}(\lambda)$ data can lead to changes influenced by variations in other optical properties not fully addressed by the models, making it difficult to attribute changes solely to biological factors. Moreover, the interdependence of retrieved parameters, such as chlorophyll, a_{CDOM} , and $b_{b,nw}$, means that errors in one can propagate to others, complicating the interpretation of these maps. For example, inaccuracies in backscatter coefficient estimates can affect chlorophyll retrievals. Additionally, variability in environmental conditions can impact the accuracy of the retrieved variables. Algorithm performance may

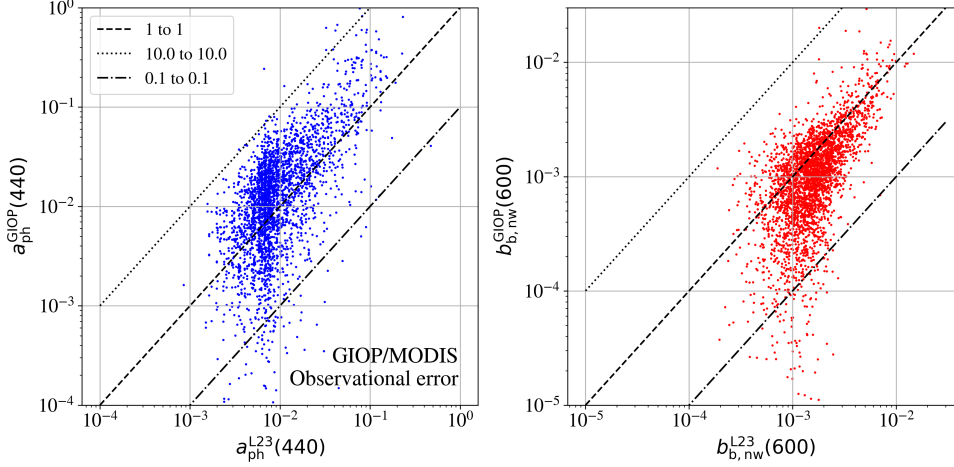


Figure 18. Retrievals of $a_{\text{ph}}(440)$ and $b_{b,nw}$ at 600 nm for the GIOP model with simulated MODIS spectra and perturbing the $R_{rs}(\lambda)$ values by the typical noise. We find the values scatter by an order of magnitude or more (and have comparable uncertainties; next section).

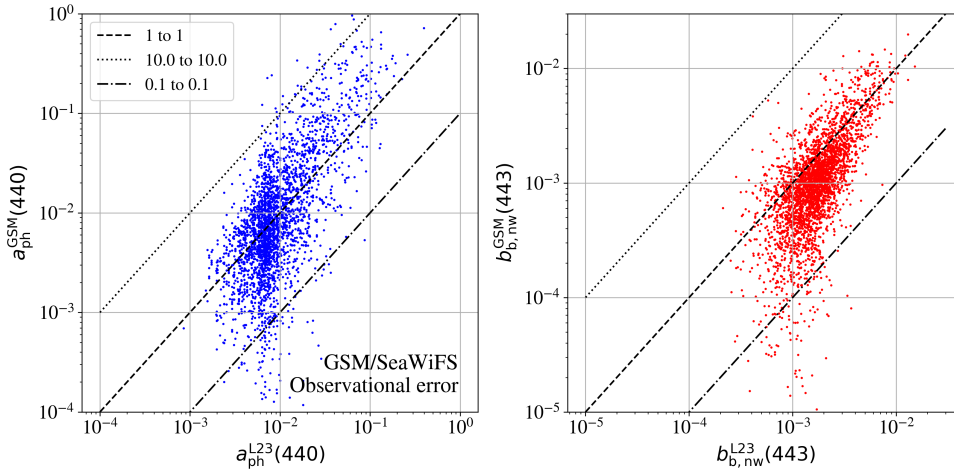


Figure 19. Same as Figure 18 but for the GSM model and simulated SeaWiFS spectra.

vary across different water types and regions, necessitating further caution in interpreting these changes.

We have also performed retrievals with GIOP on simulated PACE spectra using the uncertainties described in Figure 5. In contrast to the results from simulated MODIS spectra (Figure 18, the retrieved $a_{\text{ph}}(440)$ and $b_{\text{bp}}(443)$ values have much reduced errors (formally, $\approx 10\%$). However, each set of estimations is biased high by several tens percent and the mean absolute error (MAE) exceeds the PACE requirements (Cetinić et al., 2018). One could, of course, reduce the bias with one of several *post hoc* corrections (e.g. modify the S_{exp} value), but this may have other, unanticipated consequences. Furthermore, we reemphasize that our analysis assumes no errors in the radiative transfer, and no uncertainties related to spatial inhomogeneity (among other issues). At present, we believe that PACE is not achieving one or more Level 1 scientific requirements (Ce-

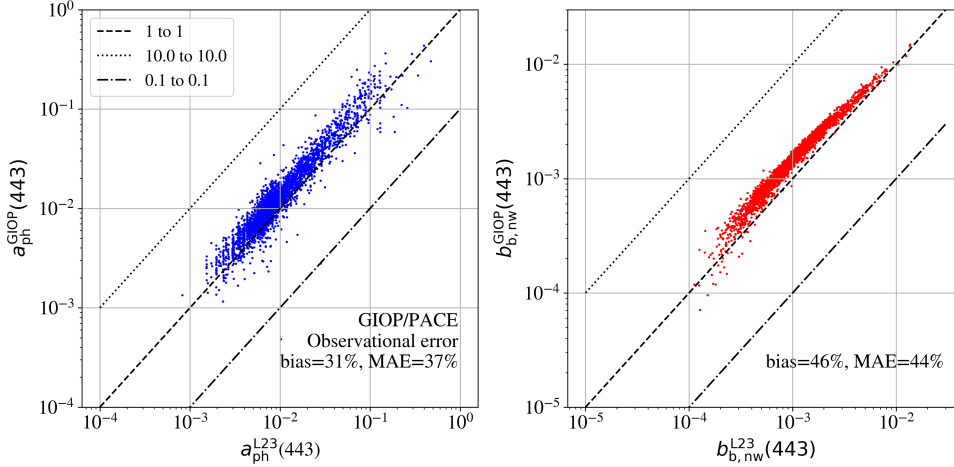


Figure 20. Same as Figure 18 but for simulated PACE spectra spectra. We note that the mean absolute errors (MAEs) estimated here for a_{ph} and b_b do meet the uncertainty requirements listed in the final PACE technical report Cetinić et al. (2018).

tiniić et al., 2018) and we are pessimistic that these may be met without including strong and strict priors from other datasets in addition to an entirely revamped methodology.

6.8 Previous Assessments

Results from tests of IOP retrieval models have been presented in multiple publications over the years since the beginning of their development (e.g. Mouw et al., 2017; Werdell et al., 2018; Seegers et al., 2018), and a discussion of all of these lies beyond the scope of this manuscript. Nevertheless, we wish to highlight one, in-depth effort summarized by the IOCCG Report 5 (Lee, 2006). Similar to our work, the participants applied their IOP retrieval algorithms to a simulated (i.e. known) dataset to assess performance. The majority of these algorithms assumed an exponential term for CDOM/detritus absorption with fixed S_{exp} and a steep value ($S_{exp} > 0.015 \text{ nm}^{-1}$). Similar to the results we found for GIOP and GSM (Figure 17,16), these consistently over-estimated $a_{ph}(\lambda)$ at 440 nm.

Only one team (Boss & Roesler) allowed S_{exp} to vary (from 0.008 to 0.023 nm^{-1}) in their algorithm which followed from the Roesler et al. (1989) publication. Referring to their Figure 8.1, one notes less biased $a_{ph}(\lambda)$ values than the other algorithms and that they were the only group to include an error estimation. Given the axes are a log-scaling, one might miss that the uncertainties in $a_{ph}(\lambda)$ are large enough to be consistent with zero. In other words, the results from the only algorithm of the report adopting S_{exp} as a free parameter showed $a_{ph}(\lambda)$ could not be positively detected from simulated data.

6.9 New Methods for Hyperspectral Data

In the context of advancing ocean color remote sensing and PACE, new algorithms have been introduced to enhance the retrieval of phytoplankton pigments using hyperspectral reflectance data (Chase et al., 2017; Kramer et al., 2022). However, these approaches face significant challenges due to the fundamental issue of $R_{rs}(\lambda)$ depending primarily on the ratio of backscattering to absorption (b_b/a) rather than on these parameters individually as emphasize in the present study. This intrinsic degeneracy means

that remote sensing reflectance alone cannot independently determine the absolute values of arbitrary non-water IOPs.

Chase et al. (2017) employ an inversion algorithm to estimate phytoplankton pigments by using the spectral shape of reflectance. Their method relies heavily on covariation relationships between chlorophyll-a and accessory pigments, which does not resolve the degeneracy problem but instead depends on pre-established statistical correlations. Furthermore, their analysis of spectral residuals shows no strong relationship between residuals and pigments, underscoring the difficulty of extracting specific pigment information from hyperspectral reflectance alone. Related, our own experiments implementing Gaussian fits to absorption spectra reveal major, insurmountable degeneracies between the components (Prochaska, 2024).

Similarly, Kramer et al. (2022) use principal components regression (PCR) modeling of the second derivative of $R_{rs}(\lambda)$ residuals to reconstruct pigment concentrations from hyperspectral data. While they claim success in modeling multiple pigments, their approach remains fundamentally limited by the same degeneracy issue. The PCR method reduces dimensionality and identifies patterns in the data, yet it still relies on the representativeness of the training dataset and may not generalize well across diverse environmental conditions. Moreover, the requirement for high spectral resolution indicates that the model’s robustness is contingent on specific sensor capabilities and noise levels, further limiting practical applications without extensive a priori data. Indeed, our experiments on derivatives of $R_{rs}(\lambda)$ reveal the uncertainties of the second derivative generally exceed the signal at all wavelengths (Prochaska, 2024).

These studies, despite their contributions, illustrate the inherent limitations of using $R_{rs}(\lambda)$ for detailed pigment retrieval without strong a priori knowledge or assumptions. Our analysis underscores the necessity of such priors to achieve accurate IOP retrievals, as $R_{rs}(\lambda)$ alone cannot provide unique solutions due to its dependence on the b_b/a ratio. Therefore, while the advancements by Chase et al. (2017) and Kramer et al. (2022) are noteworthy, their methodologies should be viewed within the context of these fundamental constraints, highlighting the need for continued refinement and incorporation of comprehensive a priori information in ocean color remote sensing algorithms.

Acknowledgments

The authors wish to thank B. Ménard, E. Boss, S. Kramer, A. Windle, H. Housekeeper, M. Zhang, and C. Mobley for discussions and/or their input on an earlier draft. We also benefited from conversations with The Astros. Last, we acknowledge deriving new insight on the problem from conversations with M. Kehrli.

References

- Behrenfeld, M. J., O’Malley, R. T., Boss, E. S., Westberry, T. K., Graff, J. R., Halsey, K. H., ... Brown, M. B. (2016, March). Revaluating ocean warming impacts on global phytoplankton. *Nature Climate Change*, 6(3), 323-330. doi: 10.1038/nclimate2838
- Bentler, P. M., & Bonett, D. G. (1980). Significance tests and goodness of fit in the analysis of covariance structures. *Psychological Bulletin*, 88(3), 588-606. doi: 10.1037/0033-2909.88.3.588
- Boss, E., Waite, A. M., Karstensen, J., Trull, T., Muller-Karger, F., Sosik, H. M., ... Wanninkhof, R. (2022). Recommendations for plankton measurements on oceansites moorings with relevance to other observing sites. *Frontiers in Marine Science*, 9. Retrieved from <https://www.frontiersin.org/journals/marine-science/articles/10.3389/fmars.2022.929436> doi: 10.3389/fmars.2022.929436

- Bricaud, A., Babin, M., Morel, A., & Claustre, H. (1995, July). Variability in the chlorophyll-specific absorption coefficients of natural phytoplankton: Analysis and parameterization. *Journal of Geophysical Research*, *100*(C7), 13,321-13,332. doi: 10.1029/95JC00463
- Bricaud, A., Morel, A., Babin, M., Allali, K., & Claustre, H. (1998, December). Variations of light absorption by suspended particles with chlorophyll a concentration in oceanic (case 1) waters: Analysis and implications for bio-optical models. *Journal of Geophysical Research*, *103*(C13), 31,033-31,044. doi: 10.1029/98JC02712
- Cael, B. B., Bisson, K., Boss, E., & Erickson, Z. r. K. (2023). How many independent quantities can be extracted from ocean color? *Limnology and Oceanography Letters*, *8*(4), 603-610. Retrieved from <https://aslopubs.onlinelibrary.wiley.com/doi/abs/10.1002/lol2.10319> doi: <https://doi.org/10.1002/lol2.10319>
- Cetinić, I., McClain, C. R., & Werdell, P. J. (2018). *PACE Technical Report Series, Volume 6: Data Product Requirements and Error Budgets* (NASA Technical Memorandum No. NASA/TM-2018 - 2018-219027/ Vol. 6). Greenbelt, MD: NASA Goddard Space Flight Center.
- Cetinić, I., Rousseaux, C. S., Carroll, I. T., Chase, A. P. ., Kramer, S. J., Werdell, P. J., ... Sayers, M. (2024). Phytoplankton composition from space: Requirements, opportunities, and challenges. *Remote Sensing of Environment*, *302*, 113964. Retrieved from <https://www.sciencedirect.com/science/article/pii/S0034425723005163> doi: <https://doi.org/10.1016/j.rse.2023.113964>
- Chase, A. P., Boss, E., Cetinić, I., & Slade, W. (2017, December). Estimation of Phytoplankton Accessory Pigments From Hyperspectral Reflectance Spectra: Toward a Global Algorithm. *Journal of Geophysical Research (Oceans)*, *122*(12), 9725-9743. doi: 10.1002/2017JC012859
- Cloern, J. E., & Jassby, A. D. (2010, March). Patterns and scales of phytoplankton variability in estuarine-coastal ecosystems. *Estuaries and Coasts*, *33*(2), 230-241. Retrieved from <https://doi.org/10.1007/s12237-009-9195-3> doi: 10.1007/s12237-009-9195-3
- Defoin-Platel, M., & Chami, M. (2007, March). How ambiguous is the inverse problem of ocean color in coastal waters? *Journal of Geophysical Research (Oceans)*, *112*(C3), C03004. doi: 10.1029/2006JC003847
- Flombaum, P., Wang, W.-L., Primeau, F. W., & Martiny, A. C. (2020, January). Global picophytoplankton niche partitioning predicts overall positive response to ocean warming. *Nature Geoscience*, *13*(2), 116-120. doi: 10.1038/s41561-019-0524-2
- Foreman-Mackey, D., Hogg, D. W., Lang, D., & Goodman, J. (2013, March). `emcee`: The mcmc hammer. *Publications of the Astronomical Society of the Pacific*, *125*(925), 306-312. Retrieved from <http://dx.doi.org/10.1086/670067> doi: 10.1086/670067
- Fox, J., Kramer, S. J., Graff, J. R., Behrenfeld, M. c. J., Boss, E., Tilstone, G., & Halsey, K. H. (2022). An absorption-based approach to improved estimates of phytoplankton bio mass and net primary production. *Limnology and Oceanography Letters*, *7*(5), 419-426. Retrieved from <https://aslopubs.onlinelibrary.wiley.com/doi/abs/10.1002/lol2.10275> doi: <https://doi.org/10.1002/lol2.10275>
- Frouin, R., & Pelletier, B. (2015, March). Bayesian methodology for inverting satellite ocean-color data. *Remote Sensing of Environment*, *159*, 332-360. doi: 10.1016/j.rse.2014.12.001
- Garver, S. A., Siegel, D. A., & B. Greg, M. (1994, September). Variability in near-surface particulate absorption spectra: What can a satellite ocean color imager see? *Limnology and Oceanography*, *39*(6), 1349-1367. doi: 10.4319/lo.1994.39.6.1349

- Gordon, H. R. (1973, December). Simple Calculation of the Diffuse Reflectance of the Ocean. *Applied Optics*, *12*(12), 2803. doi: 10.1364/AO.12.002803
- Gordon, H. R. (1986, August). Distribution Of Irradiance On The Sea Surface Resulting From A Point Source Imbedded In The Ocean. In *Society of photo-optical instrumentation engineers (spie) conference series* (Vol. 637, p. 66-71). doi: 10.1117/12.964216
- Gordon, H. R., & Morel, A. Y. (1983). *Remote assessment of ocean color for interpretation of satellite visible imagery* (Vol. 4). Springer-Verlag. (Online ISBN: 9781118663707) doi: 10.1029/LN004
- Hansen, J. E. (1971, November). Multiple Scattering of Polarized Light in Planetary Atmospheres Part II. Sunlight Reflected by Terrestrial Water Clouds. *Journal of the Atmospheric Sciences*, *28*(8), 1400-1426. doi: 10.1175/1520-0469(1971)028<1400:MSOPLI>2.0.CO;2
- Hooker, S. B., Matsuoka, A., Kudela, R. M., Yamashita, Y., Suzuki, K., & Houskeeper, H. F. (2020, January). A global end-member approach to derive $a_{CDOM}(440)$ from near-surface optical measurements. *Biogeosciences*, *17*(2), 475-497. doi: 10.5194/bg-17-475-2020
- Hovis, W. A., Clark, D. K., Anderson, F., Austin, R. W., Wilson, W. H., Baker, E. T., ... Yentsch, C. S. (1980, October 3). Nimbus-7 coastal zone color scanner: System description and initial imagery. *Science*, *210*(4465), 60-63. doi: 10.1126/science.210.4465.60
- Kramer, S. J., Siegel, D. A., Maritorena, S., & Catlett, D. (2022, March). Modeling surface ocean phytoplankton pigments from hyperspectral remote sensing reflectance on global scales. *Remote Sensing of Environment*, *270*, 112879. doi: 10.1016/j.rse.2021.112879
- Kudela, R. M., Hooker, S. B., Houskeeper, H. F., & McPherson, M. (2019, September). The Influence of Signal to Noise Ratio of Legacy Airborne and Satellite Sensors for Simulating Next-Generation Coastal and Inland Water Products. *Remote Sensing*, *11*(18), 2071. doi: 10.3390/rs11182071
- Lee, Z. (2006). *Remote sensing of inherent optical properties: Fundamentals, tests of algorithms, and applications* (IOCCG Report No. 5). Dartmouth, Canada: International Ocean-Colour Coordinating Group (IOCCG). (An Affiliated Program of the Scientific Committee on Oceanic Research (SCOR) and An Associate Member of the Committee on Earth Observation Satellites (CEOS))
- Lee, Z., Carder, K. L., & Arnone, R. A. (2002, September). Deriving inherent optical properties from water color: a multiband quasi-analytical algorithm for optically deep waters. *Applied Optics*, *41*(27), 5755-5772. doi: 10.1364/AO.41.005755
- Lee, Z., Carder, K. L., & Arnone, R. A. (2002, Sep). Deriving inherent optical properties from water color: a multiband quasi-analytical algorithm for optically deep waters. *Appl. Opt.*, *41*(27), 5755-5772. Retrieved from <https://opg.optica.org/ao/abstract.cfm?URI=ao-41-27-5755> doi: 10.1364/AO.41.005755
- Loisel, H., Schaffer Ferreira Jorge, D., Reynolds, R. A., & Stramski, D. (2023, August). A synthetic optical database generated by radiative transfer simulations in support of studies in ocean optics and optical remote sensing of the global ocean. *Earth System Science Data*, *15*(8), 3711-3731. doi: 10.5194/essd-15-3711-2023
- Loisel, H., & Stramski, D. (2000, June). Estimation of the Inherent Optical Properties of Natural Waters from the Irradiance Attenuation Coefficient and Reflectance in the Presence of Raman Scattering. *Applied Optics*, *39*(18), 3001-3011. doi: 10.1364/AO.39.003001
- Loisel, H., Stramski, D., Dessailly, D., Jamet, C., Li, L., & Reynolds, R. A. (2018, March). An Inverse Model for Estimating the Optical Absorption and Backscattering Coefficients of Seawater From Remote-Sensing Reflectance Over a Broad Range of Oceanic and Coastal Marine Environments. *Journal of Geophysical*

- Research (Oceans)*, 123(3), 2141-2171. doi: 10.1002/2017JC013632
- Maritorena, S., & Siegel, D. A. (2005, February). Consistent merging of satellite ocean color data sets using a bio-optical model. *Remote Sensing of Environment*, 94(4), 429-440. doi: 10.1016/j.rse.2004.08.014
- Maritorena, S., Siegel, D. A., & Peterson, A. R. (2002, May). Optimization of a semianalytical ocean color model for global-scale applications. *Applied Optics*, 41(15), 2705-2714. doi: 10.1364/AO.41.002705
- Mason, J. D., Cone, M. T., & Fry, E. S. (2016, Sep). Ultraviolet (250–550 nm) absorption spectrum of pure water. *Appl. Opt.*, 55(25), 7163–7172. Retrieved from <https://opg.optica.org/ao/abstract.cfm?URI=ao-55-25-7163> doi: 10.1364/AO.55.007163
- Mobley, C. D., & Sundman, L. K. (2013). *Hydrolight 5.2 ecolight 5.2 users' guide* (Tech. Rep.). Sequoia Scientific, Inc. Retrieved from <https://www.sequoiasci.com/wp-content/uploads/2013/07/HE52UsersGuide.pdf>
- Mobley, C. D. e. (2022). *The oceanic optics book*. Dartmouth, NS, Canada: International Ocean Colour Coordinating Group (IOCCG). doi: <http://dx.doi.org/10.25607/OBP-1710>
- Mouw, C. B., Hardman-Mountford, N. J., Alvain, S., Bracher, A., Brewin, R. J. W., Bricaud, A., ... Uitz, J. i. (2017). A consumer's guide to satellite remote sensing of multiple phytoplankton groups in the global ocean. *Frontiers in Marine Science*, 4. Retrieved from <https://www.frontiersin.org/journals/marine-science/articles/10.3389/fmars.2017.00041> doi: 10.3389/fmars.2017.00041
- NASA Goddard Space Flight Center. (2024). *Seabass validation search*. https://seabass.gsfc.nasa.gov/search/?search_type=Perform%20Validation%20Search&val_sata=1&val_products=11&val_source=0. (Accessed: 2024-06)
- Prochaska, J. X. (2024, January). *ocean-colour/bing: Submitted to Nature Comm*. Zenodo. Retrieved from <https://doi.org/10.5281/zenodo.13292701> doi: 10.5281/zenodo.13292701
- Prochaska, J. X., & Gray, P. (2024, June). On the fundamental additive modes of ocean color absorption. *Limnology & Oceanography*. Retrieved from <http://dx.doi.org/10.22541/essoar.171828481.15444713/v1> doi: 10.22541/essoar.171828481.15444713/v1
- Roesler, C. S., Perry, M. J., & Carder, K. L. (1989, December). Modeling in situ phytoplankton absorption from total absorption spectra in productive inland marine waters. *Limnology and Oceanography*, 34(8), 1510-1523. doi: 10.4319/lo.1989.34.8.1510
- Seegers, B. N., Stumpf, R. P., Schaeffer, B. A., Loftin, K. A., & Werdell, P. J. (2018, March). Performance metrics for the assessment of satellite data products: an ocean color case study. *Optics Express*, 26(6), 7404. doi: 10.1364/OE.26.007404
- Siegel, D. A., Behrenfeld, M. J., Maritorena, S., McClain, C. R., Antoine, D., Bailey, S. W., ... Yoder, J. A. (2013, August). Regional to global assessments of phytoplankton dynamics from the SeaWiFS mission. *Remote Sensing of Environment*, 135, 77-91. doi: 10.1016/j.rse.2013.03.025
- Stramski, D., Bricaud, A., & Morel, A. (2001, June). Modeling the Inherent Optical Properties of the Ocean Based on the Detailed Composition of the Planktonic Community. *Applied Optics*, 40(18), 2929-2945. doi: 10.1364/AO.40.002929
- Stramski, D., Joshi, I., & Reynolds, R. A. (2022, February). Ocean color algorithms to estimate the concentration of particulate organic carbon in surface waters of the global ocean in support of a long-term data record from multiple satellite missions. *Remote Sensing of Environment*, 269, 112776. doi: 10.1016/j.rse.2021.112776
- Sydor, M., Gould, R. W., Arnone, R. A., Haltrin, V. I., & Goode, W. (2004, April). Uniqueness in Remote Sensing of the Inherent Optical Properties of Ocean Water.

- Applied Optics*, 43(10), 2156-2162. doi: 10.1364/AO.43.002156
- Twardowski, M. S., Jamet, C., & Loisel, H. (2018, May). Analytical model to derive suspended particulate matter concentration in natural waters by inversion of optical attenuation and backscattering. In W. W. Hou & R. A. Arnone (Eds.), *Ocean sensing and monitoring x* (Vol. 10631, p. 106310H). doi: 10.1117/12.2309995
- Werdell, P. J., & Bailey, S. W. (2002). *The SeaWiFS bio-optical archive and storage system (SeaBASS): Current architecture and implementation* (NASA Tech. Memo. No. 2002-211617). Greenbelt, Maryland: NASA Goddard Space Flight Center.
- Werdell, P. J., Franz, B. A., Bailey, S. W., Feldman, G. C., Boss, E., Brando, V. E., ... Mangin, A. (2013, April). Generalized ocean color inversion model for retrieving marine inherent optical properties. *Applied Optics*, 52(10), 2019. doi: 10.1364/AO.52.002019
- Werdell, P. J., McKinna, L. I. W., Boss, E., Ackleson, S. G., Craig, S. E., Gregg, W. W., ... Zhang, X. (2018, January). An overview of approaches and challenges for retrieving marine inherent optical properties from ocean color remote sensing. *Progress in Oceanography*, 160, 186-212. doi: 10.1016/j.pocean.2018.01.001
- Wolanin, A., Rozanov, V. V., Dinter, T., Noël, S., Vountas, M., Burrows, J. P., & Bracher, A. (2015, September). Global retrieval of marine and terrestrial chlorophyll fluorescence at its red peak using hyperspectral top of atmosphere radiance measurements: Feasibility study and first results. *Remote Sensing of Environment*, 166, 243-261. doi: 10.1016/j.rse.2015.05.018
- Zege, E. P., Ivanov, A. P., & Katsev, I. L. (1991). *Image transfer through a scattering medium*. Springer-Verlag.
- Zhang, M., Ibrahim, A., Franz, B. A., & and Andrew M. Sayer, Z. A. (2022, Aug). Estimating pixel-level uncertainty in ocean color retrievals from modis. *Opt. Express*, 30(17), 31415-31438. Retrieved from <https://opg.optica.org/oe/abstract.cfm?URI=oe-30-17-31415> doi: 10.1364/OE.460735